

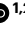



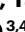
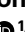










# Large-scale generation of iNK and CAR-iNK cells from CD34<sup>+</sup> haematopoietic stem and progenitor cells for adoptive immunotherapy

Received: 2 August 2024

Accepted: 27 August 2025

Published online: 07 October 2025

 Check for updates

Fangxiao Hu <sup>1,2,8</sup>, Jianhuan Li <sup>1,3,4,8</sup>, Yao Wang <sup>1,3,4,8</sup>, Yunqing Lin <sup>1,4,8</sup>, Jingliao Zhang <sup>5,8</sup>, Jiacheng Xu <sup>1,4</sup>, Xiujuan Zheng <sup>1,3,4</sup>, Qitong Weng <sup>1</sup>, Xiaofei Liu <sup>3</sup>, Yang Geng <sup>3</sup>, Hongling Wu <sup>3</sup>, Lijuan Liu <sup>1,2</sup>, Huan Peng <sup>3,4</sup>, Bingyan Wu <sup>3,4</sup>, Dehao Huang <sup>1,2</sup>, Chengxiang Xia <sup>1,2</sup>, Tongjie Wang <sup>1,2</sup>, Xin Du <sup>6</sup>, Hui Zeng <sup>7</sup>, Fang Dong <sup>5</sup>, Yingchi Zhang <sup>5</sup>, Xiaofan Zhu <sup>5</sup>✉, Mengyun Zhang <sup>1,2</sup>✉ & Jinyong Wang <sup>1,2,3,4</sup>✉

Chimaeric antigen receptor (CAR) natural killer (CAR-NK) cells are a promising alternative to CAR-T cells for immunotherapies. High and multiple doses of CAR-NK cell infusions are essential to maintain therapeutic efficacy in clinical trials, requiring efficient methods for generating CAR-NK cells at scale. Here we develop a three-step strategy to generate high yields of induced NK (iNK) and CAR-iNK cells from human umbilical cord blood CD34<sup>+</sup> haematopoietic stem and progenitor cells (CD34<sup>+</sup> HSPCs). Starting from a single umbilical cord blood unit of CD34<sup>+</sup> HSPCs, our method produces 14–83 million mature iNK cells or 7–32 million CAR-iNK cells with high expression levels of CD16 and CAR and undetectable T-cell contamination. Both fresh and thawed iNK and CAR-iNK cells demonstrate anti-tumour activities against various human cancer cells and prolong the survival of human tumour-bearing animals. The high yields of CAR-NK cells and reduced costs of our method's CAR engineering support the broad applications of these cells for treating cancer patients.

Cellular immunotherapy, particularly chimaeric antigen receptor (CAR)-T-cell therapy, has revolutionized the treatment of B-cell malignancies. Despite the remarkable efficacy of CAR-T cells, their high costs and limited cell sources have spurred interest in developing natural killer (NK) cells as an alternative to universal cellular immunotherapy<sup>1–3</sup>. NK cells have the inherent ability to directly kill neoplastic, virally infected and certain stressed cells due to abnormal expression of NK cell ligands such as major histocompatibility complex (MHC) class I and MHC class I-like molecules<sup>4</sup>. CAR-NK cell therapy is promising in achieving dual targeting and universal non-specific killing effects in treating tumours with low health risks<sup>5</sup>.

Human NK cells have a physiological turnover time of ~2 weeks in blood circulation<sup>6</sup>. The persistence of allogeneic NK cells in patients ranges from a few days to a few weeks, with an average of 7 days in most clinical trials<sup>7</sup>. New methods are needed to generate abundant CAR-NK cells and reduce CAR engineering costs, considering the high dose (10<sup>7</sup> cells per kg) and multiple dose requirement for CAR-NK cell therapy in clinical trials to enhance efficacies<sup>8,9</sup>.

CD34<sup>+</sup> haematopoietic stem and progenitor cells (HSPCs) can differentiate into multilineage blood and immune cells, including NK cells. A cytokine-based culture system has produced mean output yields of 1,879–4,450 NK cells from single HSPCs. However, at the end

A full list of affiliations appears at the end of the paper. ✉e-mail: [xfzhu@ihcams.ac.cn](mailto:xfzhu@ihcams.ac.cn); [zhangmengyun@ioz.ac.cn](mailto:zhangmengyun@ioz.ac.cn); [wangjinyong@ioz.ac.cn](mailto:wangjinyong@ioz.ac.cn)

of the culture, HSPC-NK cells express deficient levels of CD16 protein ( $3.0 \pm 2.4\%$ )<sup>10</sup>, indicating low antibody-dependent cellular cytotoxicity (ADCC) activity in the engagement of adaptive immune cells<sup>11</sup>. Previous reports proved that engineered CAR-HSPCs can also generate CAR-NK cells both *in vitro* and *in vivo*<sup>12,13</sup>.

CD34<sup>+</sup> HSPC culture and expansion techniques have advanced over the decades<sup>14,15</sup>. Artificial organoid aggregates combining seed cells with feeder cells significantly increase the generation efficiencies of induced T cells and NK cells from stem and progenitor cells<sup>16,17</sup>. Therefore, integrating HSPC expansion and organoid induction can further promote the efficiency of NK cell generation from CD34<sup>+</sup> HSPCs.

This study introduces a comprehensive method to potentially derive trillions of iNK and CAR-iNK cells from a single umbilical cord blood unit of CD34<sup>+</sup> HSPCs. This method includes three steps: CD34<sup>+</sup> HSPC expansion (days 0–14), NK lineage differentiation through organoid aggregates (days 14–28), and maturation of NK cells and large-scale proliferation in cell culture bags (days 28–49). Interestingly, a single CD34<sup>+</sup> cell ultimately produced  $1.4 \times 10^7 \pm 0.1 \times 10^7$  (henceforth, all values with measures of variation refer to mean  $\pm$  s.d.) iNK cells and  $7.6 \times 10^6 \pm 1.2 \times 10^6$  CD19 CAR-iNK cells on day 42, and much higher yields of iNK cells ( $8.3 \times 10^7 \pm 0.7 \times 10^7$ ) and CD19 CAR-iNK cells ( $3.2 \times 10^7 \pm 0.2 \times 10^7$ ) on day 49 using our technique, which increased iNK cell generation efficiency to 6,918–20,224 times over the previous method. In calculation, a single umbilical cord blood unit of CD34<sup>+</sup> HSPCs has the potential to produce trillions of CD19 CAR-iNK cells using our technique. Interestingly, our method sharply reduces the amounts of retroviral vectors to 1/140,000–1/600,000 compared to the conventional approaches of engineering CARs into mature NK cells. iNK cells and CD19 CAR-iNK cells, including thawed cells from cryopreserved conditions, show ideal immune activities and solid tumour eradication abilities for 6 months. Our method strongly supports the translational prospects for democratizing affordable CAR-iNK cell therapy for the general treatment of patients.

## Results

### Efficient generation of iNK cells and CD19 CAR-iNK cells from CD34<sup>+</sup> HSPCs

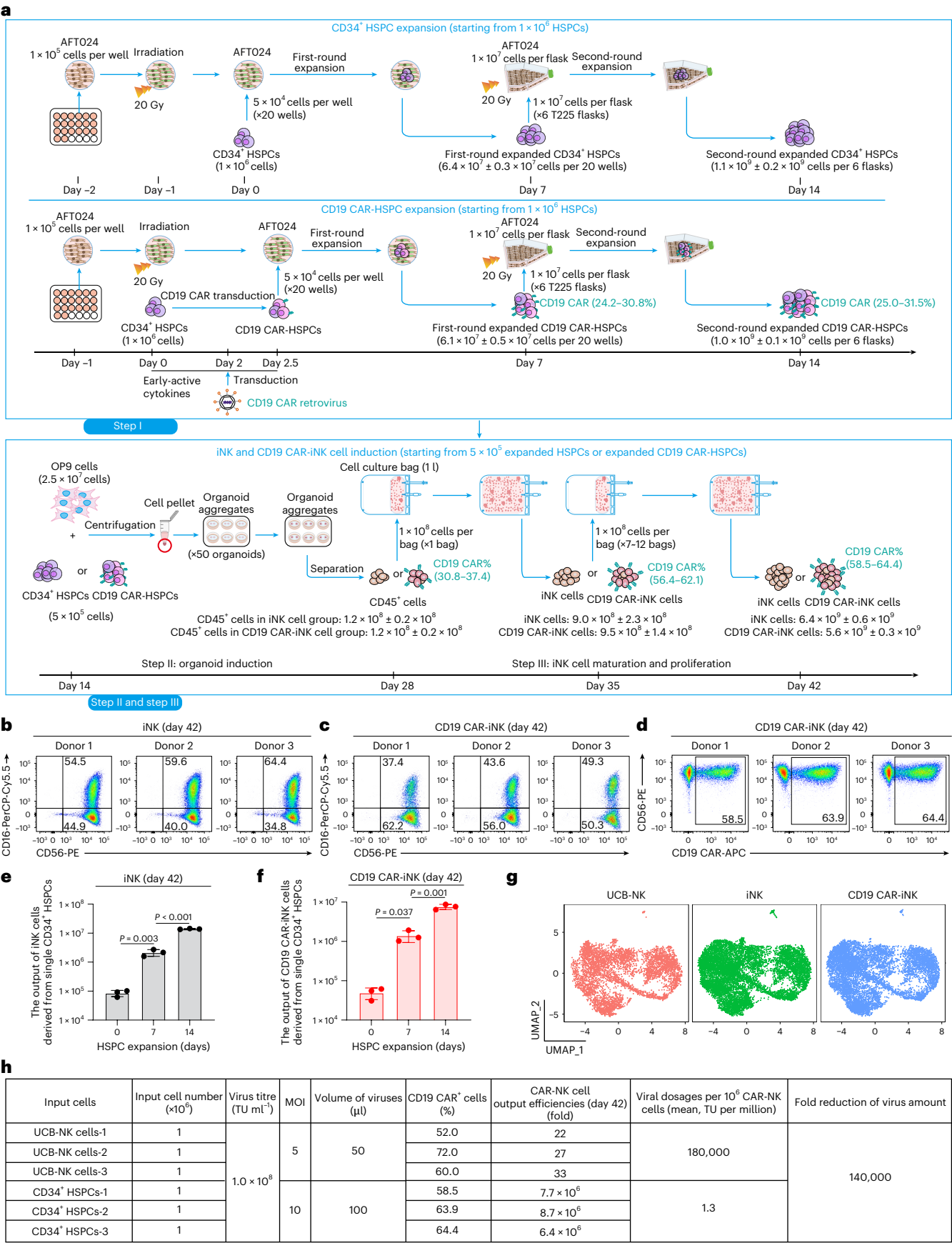
We developed a three-step culture system to generate millions of human iNK and CAR-iNK cells from a single umbilical cord blood CD34<sup>+</sup> HSPC. This system integrates strategies of HSPC expansion (step I), organoid induction (step II), and NK cell maturation and proliferation (step III) (Fig. 1a and Extended Data Fig. 1a). To generate CAR-iNK cells, we employed an SFG retroviral vector<sup>18,19</sup> to express the CAR-CD8 $\alpha$  Hinge-CD8 $\alpha$  TM-CD3 $\zeta$  (SFG-CD19 CAR) CD19 CAR cassette (Extended Data Fig. 1b and Supplementary Table 1). To reduce the cost of CAR engineering, we transduced SFG-CD19 CAR retroviral vectors in the primary CD34<sup>+</sup> HSPC stage before any expansion, rather than in the mature NK stage. CD34<sup>+</sup> HSPCs were initially stimulated for 48 h and then transduced with CD19 CAR retroviral vectors at a multiplicity

of infection (MOI) of 10 through spin infection. At 12 h after infection, the transduced CD34<sup>+</sup> HSPCs were immediately used for expansion culture. To enormously expand CD34<sup>+</sup> HSPCs and CD19 CAR CD34<sup>+</sup> HSPCs (CD19 CAR-HSPCs), we established an expansion system using AFT024 cells as feeders and the HSC culture formula<sup>20–22</sup>. In detail, we seeded AFT024 cells ( $1 \times 10^5$  cells per well, 20 wells) in a 24-well plate, followed by irradiation (20 Gy) to arrest feeder growth. CD34<sup>+</sup> HSPCs or CD19 CAR-HSPCs ( $5 \times 10^4$  cells per well, 20 wells) were seeded in irradiated AFT024 cells for the first round of 7-day expansion in the presence of HSC culture medium<sup>15,23</sup>. After the first round of expansion, all cells were collected and seeded equally into 6 flasks ( $1 \times 10^7$  cells per flask) containing irradiated AFT024 cells for the second round of 7-day expansion in the presence of HSC culture medium. To efficiently drive differentiation of the NK lineage from CD34<sup>+</sup> HSPC, we used the organoid aggregate induction method we established previously<sup>17</sup>. We combined  $5 \times 10^5$  expanded CD34<sup>+</sup> HSPCs or CD19 CAR-HSPCs with  $2.5 \times 10^7$  OP9 cells to form 50 organoids ( $1 \times 10^4$  expanded CD34<sup>+</sup> HSPCs or CD19 CAR-HSPCs and  $5 \times 10^5$  OP9 cells per organoid aggregate). These organoids were seeded in transwells, followed by a 14-day induction of the NK lineage. On day 28, all organoids on the membrane were digested into single cells, which were immediately transferred to a 1 l cell culture bag (50 organoid-derived single CD45<sup>+</sup> cells per bag,  $\sim 1 \times 10^8$  cells per bag) for a 7-day culture to achieve maturation and proliferation of iNK cells. On day 35, all cells in the cell culture bag were collected and distributed into multiple cell culture bags ( $1 \times 10^8$  cells per bag) for another 7 days of proliferation of iNK cells or CAR-iNK cells.

With the three-step culture system, we successfully collected mature iNK cells and CD19 CAR-iNK cells on day 42 with >99.0% purity (CD45<sup>+</sup>CD56<sup>+</sup>CD16<sup>+/–</sup>), and high expression levels of CD16 (37.4%–69.4%) signalled the functional maturation of NK cells possessing antibody-dependent cytotoxicity<sup>17</sup> (Fig. 1b,c and Extended Data Fig. 1c). The ratios of CD19 CAR-positive iNK cells derived from three independent donor CD34<sup>+</sup> HSPCs after CAR engineering were 58.5%, 63.9% and 64.4%, with an average of  $62.3 \pm 3.3\%$  (Fig. 1d). The vector copy number (VCN) in CD19 CAR-expressing iNK cells (CD19 CAR-iNK) is  $4.6 \pm 0.1$ , which did not differ from that of same-donor-generated CD19 CAR-UCB-NK cells ( $4.7 \pm 0.4$ ) (Extended Data Fig. 1d). Moreover, we adopted a previously described methodology<sup>24</sup> to evaluate the tonic signalling in CD19 CAR-iNK cells. The CD19 CAR-iNK cells exhibited higher tonic signalling compared with same-donor-generated truncated CD19 CAR-expressing UCB-NK cells (CD19CAR-without CD3 $\zeta$ -UCB-NK). The tonic signalling strength in CD19 CAR-iNK cells and same-donor-generated CD19 CAR-UCB-NK cells were comparable (Extended Data Fig. 1e). In calculation, single CD34<sup>+</sup> HSPCs without expansion (day 0) produce  $8.5 \times 10^4 \pm 2.1 \times 10^4$  iNK cells and  $4.9 \times 10^4 \pm 1.6 \times 10^4$  CD19 CAR-iNK cells ( $n = 3$ ). Single CD34<sup>+</sup> HSPCs that undergo 7-day expansion (day 7) produce  $2.1 \times 10^6 \pm 0.6 \times 10^6$  iNK cells and  $1.4 \times 10^6 \pm 0.5 \times 10^6$  CD19 CAR-iNK cells ( $n = 3$ ). Furthermore, single CD34<sup>+</sup> HSPCs undergoing 14-day expansion (day 14) produce

**Fig. 1 | A three-step strategy for generating iNK cells and CD19 CAR-iNK cells from CD34<sup>+</sup> HSPCs.** **a**, Schematic diagram showing the generation of iNK cells and CD19 CAR-iNK cells from CD34<sup>+</sup> HSPCs or CD19 CAR-HSPCs. Step I involves the expansion of CD34<sup>+</sup> HSPCs or CD19 CAR CD34<sup>+</sup> HSPCs. AFT024 cells ( $1 \times 10^5$  cells per well) were seeded in 24-well plates and then irradiated (20 Gy). CD34<sup>+</sup> HSPCs or CD19 CAR-HSPCs ( $5 \times 10^4$  cells per well) were seeded on the irradiated AFT024 cells and co-cultured for the first round. On day 7, CD34<sup>+</sup> HSPCs or CD19 CAR-HSPCs from the first-round expansion were collected and seeded in the new irradiated AFT024 cells ( $1 \times 10^7$  cells per flask) for the second-round expansion. Step II involves the differentiation of the NK lineage using the organoid aggregate induction method. CD34<sup>+</sup> HSPCs or CD19 CAR-HSPCs ( $1 \times 10^4$  cells per organoid) collected from step I were combined with OP9 cells ( $5 \times 10^5$  cells per organoid) to prepare organoid aggregates, which were seeded in transwells and cultured for 14 days for induction of iNK cells or CD19 CAR-iNK cells. Step III involves the maturation and proliferation of NK cells. CD45<sup>+</sup> cells collected from step II were

transferred to cell culture bags and cultured for 14 days. **b,c**, Flow cytometric analysis of the immune phenotypes (CD56<sup>+</sup>CD16<sup>+/–</sup>) of iNK cells (**b**) and CD19 CAR-iNK cells (**c**). Data were collected from 3 donor umbilical cord blood units. **d**, Flow cytometric analysis of CD19 CAR expression in CD19 CAR-iNK cells. **e,f**, Statistical analysis of the output efficiencies of iNK cells (CD45<sup>+</sup>CD3<sup>+</sup>CD56<sup>+</sup>CD16<sup>+/–</sup>;  $n = 3$  donor umbilical cord blood units per group (**e**)) or CD19 CAR-iNK cells (CD45<sup>+</sup>CD3<sup>+</sup>CD56<sup>+</sup>CD16<sup>+/–</sup>CD19 CAR<sup>+</sup>;  $n = 3$  donor umbilical cord blood units per group (**f**)) on day 42, derived from single CD34<sup>+</sup> HSPCs. Day 0, fresh CD34<sup>+</sup> HSPCs. Day 7, 7-day expanded CD34<sup>+</sup> HSPCs. Day 14, 14-day expanded CD34<sup>+</sup> HSPCs. Data are shown as mean  $\pm$  s.d. of independent biological replicates. *P* values were calculated using unpaired two-sided *t*-test. Exact *P* values are labelled. **g**, UMAP visualization of UCB-NK cells, iNK cells and CD19 CAR-iNK cells. **h**, Table showing the calculated quantities of CD19 CAR retroviruses (TU). The viral particles required to generate  $1.0 \times 10^6$  CD19 CAR-iNK cells and CD19 CAR-UCB-NK cells were compared.





$1.4 \times 10^7 \pm 0.1 \times 10^7$  iNK cells and  $7.6 \times 10^6 \pm 1.2 \times 10^6$  CD19 CAR-iNK cells ( $n = 3$ ) (Fig. 1e,f). A 14-day CD34<sup>+</sup> cell expansion step resulted in eventual output efficiencies of iNK cells and CD19 CAR-iNK cells of >160 times compared to fresh HSPCs. Single-cell RNA-seq analysis demonstrated that most iNK and CD19 CAR-iNK cells projected well to activated NK cells from human umbilical cord blood (UCB-NK cells) (Fig. 1g). We also performed differential expression analysis among the three distinct NK cells. The upregulated genes in iNK cells compared to UCB-NK cells were enriched in pathways related to immune effector regulation (Extended Data Fig. 2a,b). The upregulated pathways in CD19 CAR-iNK cells compared to iNK cells were associated with lymphoid differentiation and T-cell activation (Extended Data Fig. 2c,d). Furthermore, we also performed transcriptome analysis among iNK cells, iPSC-iNK cells (HRA001609)<sup>17</sup>, ESC-iNK cells (HRA001609)<sup>17</sup> and UCB-NK cells. Interestingly, uniform manifold approximation and projection (UMAP) analysis revealed that iNK cells clustered closely with primary UCB-NK cells, whereas iPSC-iNK and ESC-iNK cells formed distinct clusters with minimal overlap with UCB-NK cells (Extended Data Fig. 2e). Gene Ontology (GO) enrichment analysis showed that genes upregulated in iNK cells compared to ESC-iNK cells or iPSC-iNK cells were enriched in pathways associated with metabolic reprogramming, immune activation and NK effector functions (Extended Data Fig. 2f–i). In addition, iNK cells and CD19 CAR-iNK cells expressed similar levels of surface marker genes of NK cells as UCB-NK cells, including activating receptor genes CD319-encoding *SLAMF7*, Nkp30-encoding *NCR3*, Nkp44-encoding *NCR2*, NKG2D-encoding *KLRK1*, *CD69*, Nkp46-encoding *NCR1*, TRAIL-encoding *TNFSF10* and FasL-encoding *FASLG*, and inhibitory receptor genes CD94-encoding *KLRD1*, NKG2A-encoding *KLRC1*, and *CD96* (Extended Data Fig. 2j). We also analysed the critical KIRs: KIR2DL1, KIR2DL3, KIR3DL1, KIR3DL2 and KIR2DS4 in iNK cells<sup>25,26</sup>. We observed differential expression patterns of inhibitory KIR repertoire among iNK cells, iPSC-iNK cells, ESC-iNK cells and natural UCB-NK cells (Extended Data Fig. 2k). Flow cytometry analysis showed that UCB-NK cells expressed a full spectrum of KIRs. Among the three types of induced NK cell, only CD34<sup>+</sup> HSPC-derived iNK cells exhibited an expression pattern of KIRs closer to that of natural UCB-NK cells. iPSC- and ESC-derived iNK cells showed weak expressions of KIRs at the protein level, including KIR2DL1, KIR2DL3, KIR3DL1 and KIR2DS4 (Extended Data Fig. 2l). To prepare 1 million CAR-NK cells, our method significantly reduced the quantities of retroviral vectors to 1/140,000 compared to conventional techniques for engineering CARs into mature NK cells<sup>27</sup> (Fig. 1h). Furthermore, iNK and CD19 CAR-iNK cells could expand slightly in a bag-based culture system for another 7 days. We collected iNK cells (Extended Data Fig. 3a) and CD19 CAR-iNK cells (Extended Data Fig. 3b) on day 49, and found that cells exhibited further increases in CD16 expression levels (iNK cell group,  $67.8 \pm 3.4\%$ , CD19 CAR-iNK cell group,  $53.5 \pm 6.2\%$ ,  $n = 3$ ) (Extended Data Fig. 3a,b), stable expression ratios of CD19 CAR in CD19 CAR-iNK cells ( $62.9 \pm 5.7\%$ ,  $n = 3$ ) (Extended Data Fig. 3c), and much higher yields of iNK cells ( $8.3 \times 10^7 \pm 0.7 \times 10^7$ ,  $n = 3$ ) (Extended Data Fig. 3d) and CD19 CAR-iNK

cells ( $3.2 \times 10^7 \pm 0.2 \times 10^7$ ,  $n = 3$ ) (Extended Data Fig. 3e). The 21-day bag-based culture further reduced the quantity of retroviral vectors to 1/600,000 when compared to conventional methods of engineering CARs into mature NK cells (Extended Data Fig. 3f).

We monitored the immune phenotypes and summarized the related ratios and cell numbers throughout the process. We first analysed the ratios of CD34<sup>+</sup> cells during the expansion step. On day 7,  $92.3 \pm 3.6\%$  (HSPC group,  $n = 3$ ) of cells retained CD45<sup>+</sup>CD34<sup>+</sup> HSPC phenotypes. Even with engineered CAR expression elements,  $86.0 \pm 2.3\%$  (CD19 CAR-HSPC group,  $n = 3$ ) of cells still maintained the CD45<sup>+</sup>CD34<sup>+</sup> HSPC phenotypes. In comparison, we did not observe significant differences in CD34 expression ratios between the HSPC group and the CD19 CAR-HSPC group after 7 days of expansion ( $P > 0.05$ ) (Fig. 2a,b). These ratios decreased to  $71.9 \pm 4.7\%$  (HSPC group,  $n = 3$ ) and  $61.0 \pm 2.4\%$  (CD19 CAR-HSPC group,  $n = 3$ ) on day 14 (Fig. 2a,b). It is noteworthy that the expression of CD19 CAR slightly decreased CD34-positive cell rates after 14 days of expansion (HSPC group vs HSPC group CD19 CAR,  $P < 0.05$ ) (Fig. 2b). Interestingly,  $1 \times 10^6$  CD34<sup>+</sup> HSPC cells resulted in  $6.4 \times 10^7 \pm 0.3 \times 10^7$  (CD34<sup>+</sup> HSPC group) and  $6.1 \times 10^7 \pm 0.5 \times 10^7$  (CD19 CAR-HSPC group) CD34<sup>+</sup> cells on day 7. A 14-day expansion further yielded  $1.1 \times 10^9 \pm 0.2 \times 10^9$  (CD34<sup>+</sup> HSPC group) and  $1.0 \times 10^9 \pm 0.1 \times 10^9$  (CD19 CAR-HSPC group) CD34<sup>+</sup> cells ( $n = 3$ ) (Figs. 1a and 2c).

To increase the efficiency of NK cell generation, we drove expanded CD34<sup>+</sup> HSPCs and CD19 CAR-HSPCs toward the NK cell lineage via an efficient organoid induction approach<sup>17</sup>. From days 14–28, the CD34<sup>+</sup> population decreased, while the proportion of cells in the NK lineage that express CD7 and CD56 gradually increased (Fig. 2d,e). On average, 50 organoids produced  $1.2 \times 10^8 \pm 0.2 \times 10^8$  CD45<sup>+</sup> cells (CD34<sup>+</sup> HSPC group) and  $1.2 \times 10^8 \pm 0.2 \times 10^8$  (CD19 CAR-HSPC group) CD45<sup>+</sup> cells, including precursor cells and NK cells, after the 2-week organoid induction (day 28) (Figs. 1a and 2f).

Subsequently, every 50 organoids as a group were digested in single-cell suspensions using collagenase type IV and dispase as previously reported<sup>17</sup>, and then transferred to commercial cell culture bags (1 l per bag) for 14-day NK cell maturation and proliferation<sup>17</sup>. After 7 days of bag culture (day 35), the NK precursor cells matured into the NK cell phenotype (CD45<sup>+</sup>CD3<sup>+</sup>CD56<sup>+</sup>), which reached  $97.0 \pm 0.2\%$  (iNK cells,  $n = 3$ ) and  $95.6 \pm 0.4\%$  (CD19 CAR-iNK cells,  $n = 3$ ) of total CD45<sup>+</sup> cells (Fig. 2g,h). After a 14-day bag culture (day 42), NK cell purity reached  $99.6 \pm 0.0\%$  (iNK cell group,  $n = 3$ ) and  $99.5 \pm 0.3\%$  (CD19 CAR-iNK cell group,  $n = 3$ ) (Fig. 2g,h). On average, single cells of 50 organoids as input produced  $6.4 \times 10^9 \pm 0.6 \times 10^9$  (iNK cell group) and  $5.6 \times 10^9 \pm 0.3 \times 10^9$  (CD19 CAR-iNK cell group) CD56<sup>+</sup> iNK cells after 2 weeks of maturation and proliferation of NK cells (Figs. 1a and 2i). To maintain the optimal activity of NK cells, we collected iNK cells and CD19 CAR-iNK cells on day 42.

Unlike the traditional NK cell expansion method using human tissue-derived NK cells as input that introduces risks of T-cell contamination, our method could not produce any T cells due to a lack of Notch signalling and IL-2. Eventually, we produced over 99.0% iNK

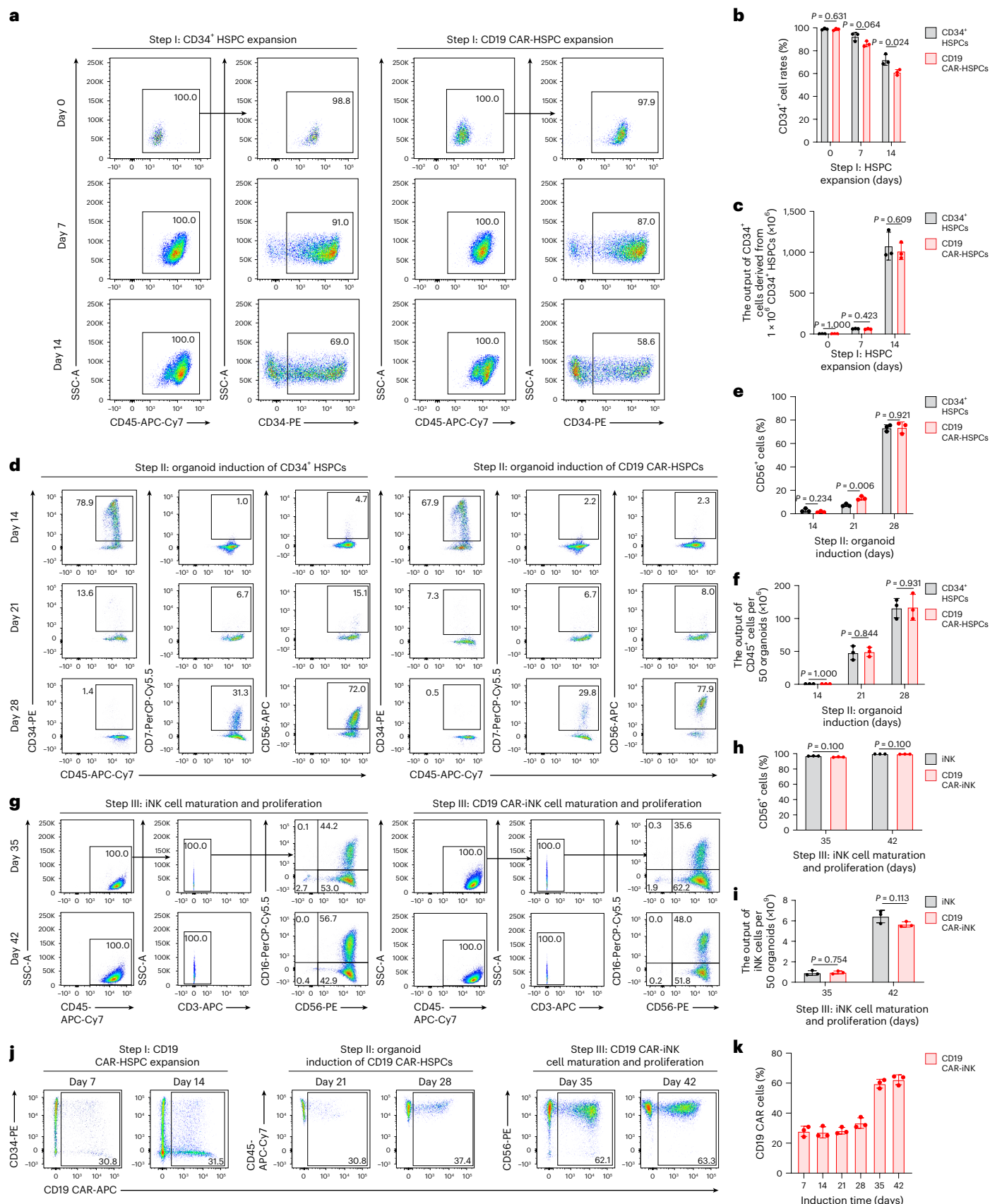
**Fig. 2 | Cellular kinetics in the three-step strategy to generate iNK cells and CD19 CAR-iNK cells.** **a**, Representative fluorescence-activated cell sorting (FACS) plots showing the ratios of CD34<sup>+</sup> HSPCs (CD45<sup>+</sup>CD34<sup>+</sup>) during expansion (step I) of CD34<sup>+</sup> HSPCs (left) and CD19 CAR-HSPCs (CD45<sup>+</sup>CD34<sup>+</sup>) (right) (day 0, day 7 and day 14). **b**, Statistical analysis of the ratios of CD45<sup>+</sup>CD34<sup>+</sup> cells in CD34<sup>+</sup> HSPCs and CD19 CAR-HSPCs (CD45<sup>+</sup>CD34<sup>+</sup>) during step I. ( $n = 3$  donor umbilical cord blood units per group). **c**, Statistical analysis of the output number of CD34<sup>+</sup> HSPCs and CD19 CAR-HSPCs derived from  $1.0 \times 10^6$  CD34<sup>+</sup> HSPCs in step I. ( $n = 3$  donor umbilical cord blood units per group). **d**, Representative FACS plots showing the ratios of CD45<sup>+</sup>CD34<sup>+</sup>, CD45<sup>+</sup>CD7<sup>+</sup> and CD45<sup>+</sup>CD56<sup>+</sup> cells of the organoid aggregates derived from CD34<sup>+</sup> HSPCs and CD19 CAR-HSPCs in step II. **e**, Statistical analysis of the ratios of CD45<sup>+</sup>CD56<sup>+</sup> cells in step II. ( $n = 3$  donor umbilical cord blood units per group). **f**, Statistical analysis of the number of CD45<sup>+</sup> cell outputs derived from 50 organoids in step II. ( $n = 3$  donor

umbilical cord blood units per group). **g**, Representative FACS plots showing the phenotypes (CD45<sup>+</sup>CD3<sup>+</sup>CD56<sup>+</sup>CD16<sup>+/−</sup>) of total cells on days 35 and 42 during cell maturation and proliferation of iNK (left) or CD19 CAR-iNK (right) (step III). **h**, Statistical analysis of the ratios of CD45<sup>+</sup>CD3<sup>+</sup>CD56<sup>+</sup> cells on days 35 and 42 in step III. ( $n = 3$  donor umbilical cord blood units per group). **i**, Statistical analysis of the output of CD45<sup>+</sup>CD3<sup>+</sup>CD56<sup>+</sup> cells derived from 50 organoids on days 35 and 42 in step III. ( $n = 3$  donor umbilical cord blood units per group). **j**, Representative FACS plots showing the expression of CD19 CAR in total cells at the indicated time points. **k**, Statistical analysis of the ratios of CD45<sup>+</sup>CD19 CAR<sup>+</sup> cells at the indicated time points. ( $n = 3$  donor umbilical cord blood units per group). Data are shown as mean  $\pm$  s.d. of independent biological replicates. *P* values were calculated using unpaired two-sided *t*-test (**b,c,e,f,i**) or two-sided Mann–Whitney *U*-test (**h**). Exact *P* values are labelled. K, thousand.



cells with zero T-cell contamination (Fig. 2g). Notably, during the bag culture period, we observed significant increases in CD16-positive iNK cells, rising from 44.2% to 56.7% (iNK cells) and 35.6% to 48.0% (CD19 CAR-iNK cells) (Fig. 2g). Subsequently, we monitored the

changes in the dynamic ratio of CD19 CAR expression throughout the CD19 CAR-iNK cell induction process. We observed comparable CD19 CAR expression ratios on day 7 ( $27.9 \pm 3.4\%$ ,  $n = 3$ ), day 14 ( $27.2 \pm 3.7\%$ ,  $n = 3$ ) and day 21 ( $28.3 \pm 2.2\%$ ,  $n = 3$ ), with a slight increase



on day 28 ( $33.4 \pm 3.5\%$ ,  $n = 3$ ) (Fig. 2j,k). Interestingly, CD19 CAR cell expression ratios increased significantly to  $59.6 \pm 2.9\%$  ( $n = 3$ ) on day 35 and reached  $62.3 \pm 3.3\%$  on day 42 ( $n = 3$ ), which were comparable to expression ratios in engineered UCB-NK cells ( $61.3 \pm 10.1\%$ ,  $n = 3$ ) (Figs. 1h and 2j,k). We observed an obvious CD19 CAR<sup>+</sup>CD34<sup>+</sup> cell population on day 14 after expansion (Fig. 2j). To confirm that these CD19 CAR<sup>+</sup>CD34<sup>+</sup> cells on day 14 were the differentiating cells derived from the CD19 CAR<sup>+</sup>CD34<sup>+</sup> population on day 4, we sorted CD19 CAR<sup>+</sup>CD34<sup>+</sup> cells on day 4 and expanded these cells for 10 days. Flow cytometry analysis confirmed that a 10-day culture resulted in 45.3% CD19 CAR<sup>+</sup>CD34<sup>+</sup> cells (Extended Data Fig. 4a,b). To investigate whether the CD19 CAR<sup>+</sup>CD34<sup>+</sup> cells on day 14 possess the capability to generate CAR-iNK cells, we sorted these cells and mixed them with sorted CD34<sup>+</sup> cells without CAR viral transduction (1:1 ratio) for iNK induction. Eventually, the CD19 CAR<sup>+</sup>CD34<sup>+</sup> cells contributed 35.6% CD19 CAR<sup>+</sup> iNK cells (Extended Data Fig. 4c,e). Of note, we also sorted CD19 CAR<sup>+</sup>CD34<sup>+</sup> cells on day 14 and mixed them 1:1 with untransduced CD34<sup>+</sup> HSPCs for iNK induction. The CD19 CAR<sup>+</sup>CD34<sup>+</sup> cells on day 14 contributed 71.9% CD19 CAR<sup>+</sup> iNK cells (Extended Data Fig. 4d,e). We observed that even the CD19 CAR<sup>+</sup>CD34<sup>+</sup> population from CD19 CAR-HSPCs on day 14 can also contribute 25.2% CAR<sup>+</sup> iNK cells (Extended Data Fig. 4f,g). The reason is that the real viral transduction efficiency at the CD34<sup>+</sup> HSPC stage is much higher than the readout using the CAR-positive rate detected by flow cytometry. The current CD19 CAR retroviral vector copy number in CD19 CAR-iNK cells approaches the FDA-recommended upper limit (VCN < 5 per transduced cell). To further reduce the CD19 CAR retroviral copy number to a much lower level and ensure high CD19 CAR cell expression ratios, we added an enrichment step for CD19 CAR<sup>+</sup>CD34<sup>+</sup> HSPCs (CD19 CAR-HSPCs) on day 7 during the HSPC expansion stage (Extended Data Fig. 5a). After a 7-day expansion of the enriched CD19 CAR-HSPCs (Extended Data Fig. 5a), we conducted iNK cell induction. The CD19 CAR-iNK cells were >90% in the final collection of iNK cells on day 42 (Extended Data Fig. 5b–f). Furthermore, the enriched CD19 CAR-HSPCs, which were transduced with the lower copy numbers of CD19 CAR retroviral vectors, can also differentiate into >90% CD19 CAR-iNK cells. The VCN is  $0.49 \pm 0.03$  per cell in total iNK cells or  $0.53 \pm 0.03$  per cell in CD19 CAR-expressing iNK cells (Extended Data Fig. 5g). Collectively, all the CD19 CAR<sup>+</sup>CD34<sup>+</sup>, CD19 CAR<sup>+</sup>CD34<sup>+</sup> and CD19 CAR<sup>+</sup>CD34<sup>+</sup> populations on day 14 can output CAR-iNK cells with differential efficiencies. CD19 CAR<sup>+</sup>CD34<sup>+</sup> cells on day 14 possess the strongest potential for generating CAR-iNK cells. This suggested that CAR expression in HSPCs enhanced the CAR-iNK generation efficiency, which is consistent with the results reported in previous work done in mice<sup>13</sup>.

Collectively, using our three-step induction strategy, single CD34<sup>+</sup> HSPCs ultimately produced  $1.4 \times 10^7 \pm 0.1 \times 10^7$  iNK cells and  $7.6 \times 10^6 \pm 1.2 \times 10^6$  CD19 CAR-iNK cells on day 42, and much higher

yields of iNK cells ( $8.3 \times 10^7 \pm 0.7 \times 10^7$ ) and CD19 CAR-iNK cells ( $3.2 \times 10^7 \pm 0.2 \times 10^7$ ) on day 49. A single umbilical cord blood unit of CD34<sup>+</sup> cells ( $>1 \times 10^6$ ) has the capacity to deliver  $\sim 1.4 \times 10^{13}$  to  $8.3 \times 10^{13}$  mature iNK or  $7.6 \times 10^{12}$  to  $3.2 \times 10^{13}$  CAR-iNK cells, which prospectively ensures 760 to 83,000 doses ( $10^9$ – $10^{10}$  cells per dose) for treating patients.

### Molecular features and immune activities of CD34<sup>+</sup> HSPC-derived iNK cells

The activation state and functionalities of NK cells are determined by the expression patterns of activating and inhibitory receptors and the secretion of cytokines and lytic granules (Fig. 3a). As expected, iNK cells expressed classical NK activating receptors, including CD319, Nkp30, Nkp44, NKG2D and CD69, and NK inhibitory receptors, including CD94, NKG2A and CD96<sup>28,29</sup>. Furthermore, iNK cells also highly expressed critical NK effector molecules, including apoptosis-related ligands TRAIL and FasL<sup>30</sup> (Fig. 3b). Subsequently, we analysed CD107a<sup>31</sup>, a typical membrane protein associated with the cytotoxic activity of NK cells, along with tumour necrosis factor (TNF)<sup>32</sup>, interferon gamma (IFN $\gamma$ ), Perforin and Granzyme B (GZMB)<sup>33</sup>. After exposure to phorbol myristate acetate (PMA)/ionomycin, all these molecules were upregulated in iNK and same-cord-blood donor-derived UCB-NK cells (Fig. 3c). Moreover, statistical analysis did not show substantial differences in protein expression patterns between UCB-NK cells and iNK cells (Fig. 3d). To further evaluate the expression of these markers after tumour stimulation, we analysed the expression levels of these proteins after K562 stimulation by flow cytometry and enzyme-linked immunosorbent assay (ELISA). CD107a, TNF, IFN $\gamma$ , GZMB and Perforin still showed similar expression patterns in iNK cells and in same-donor expanded UCB-NK cells (Extended Data Fig. 6a–c).

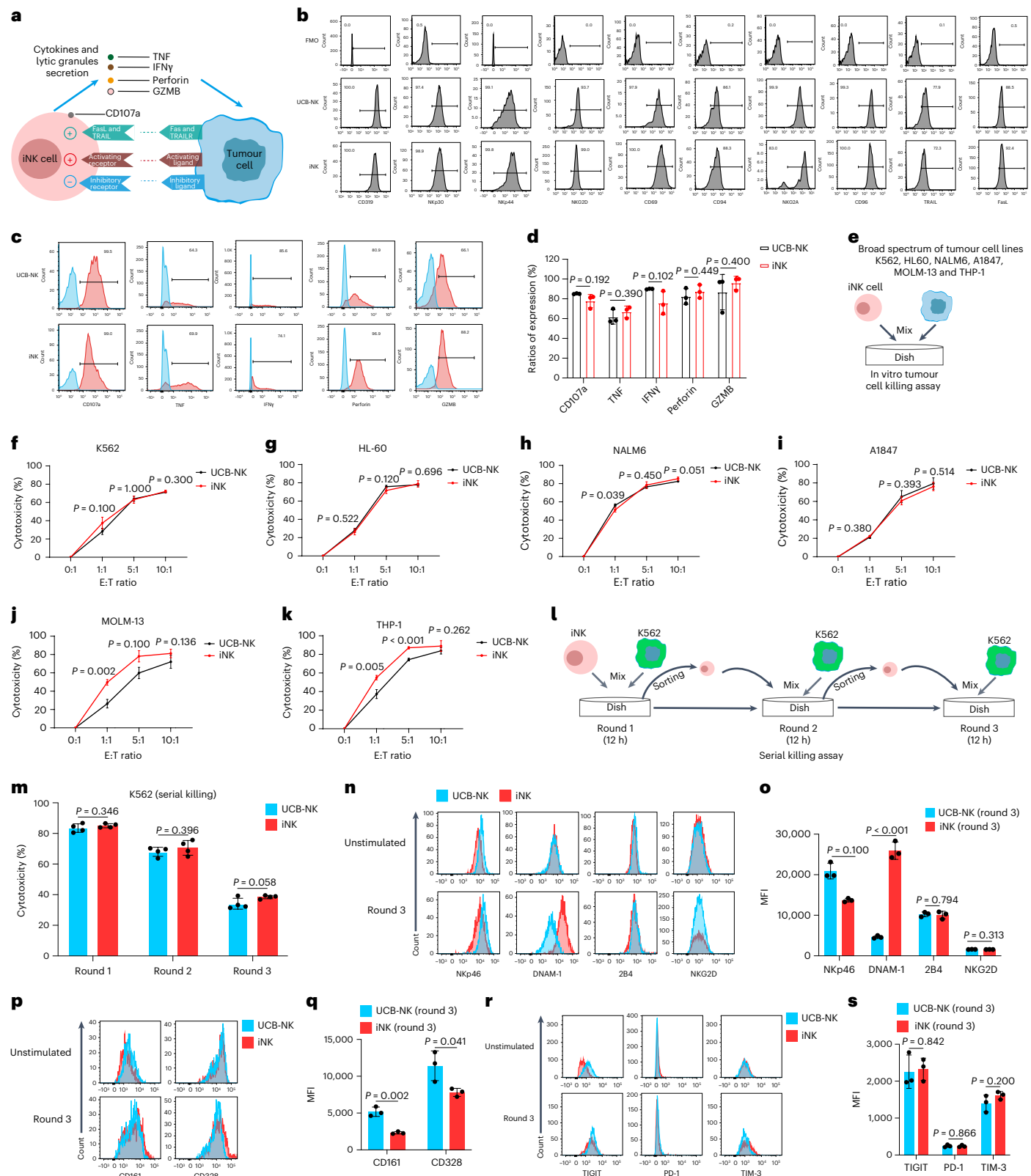
Unlike adaptive T cells, NK cells possess an innate ability to recognize and eliminate tumour cells exhibiting reduced MHC class I expression<sup>34</sup>. Therefore, we first evaluated the tumouricidal capacity of iNK cells using various cancer cell lines, including the human erythroleukaemia cell line K562, the human Caucasian promyelocytic leukaemia cell line HL-60, the human B lymphoblastic leukaemia cell line NALM6, the human ovarian cancer cell line A1847, the human acute myeloid leukaemia cell line MOLM-13 and the Epstein–Barr virus-negative B-cell lymphoma cell line THP-1 (Fig. 3e). iNK cells showed tumour killing activities similar to those of UCB-NK cells expanded from the same cord-blood donor (Fig. 3f–k). At lower effector to target (E:T) ratios, iNK cells exhibited superior cytotoxicity against MOLM-13 and THP-1 (Fig. 3h,j,k). To evaluate the persistent cytotoxic activity of iNK cells, we employed a previously reported method<sup>35</sup> to perform serial tumour-killing assays using K562 tumour cells at an E:T ratio of 1:1 (Fig. 3l). iNK cells consistently demonstrated persistent cytotoxicity against K562 cells in all three rounds of killing, similar to the observation for UCB-NK cells expanded from the same

**Fig. 3 | Molecular features and immune activities of CD34<sup>+</sup> HSPC-derived iNK cells.** **a**, Schematic diagram showing the mechanisms by which iNK cells recognize and kill tumour cells. **b**, Flow cytometric analysis of typical NK receptors and effectors (CD319, Nkp30, Nkp44, NKG2D, CD69, CD94, NKG2A, CD96, TRAIL, FasL) in iNK cells and in same-donor expanded UCB-NK cells (CD45<sup>+</sup>CD56<sup>+</sup>). FMO, fluorescence minus one. **c**, Representative flow cytometry histograms showing the expression levels of CD107a, TNF, IFN $\gamma$ , Perforin and GZMB proteins in iNK cells and in same-donor expanded UCB-NK cells (CD45<sup>+</sup>CD56<sup>+</sup>). **d**, Statistical analysis of expression levels of CD107a, TNF, IFN $\gamma$ , Perforin and GZMB proteins ( $n = 3$  in each group). **e**, Schematic diagram of the measurement of non-specific cytotoxicities of iNK cells. **f–k**, Statistical analysis of non-specific cytotoxicities of iNK cells ( $n = 3$  per group) and of same-donor expanded UCB-NK cells ( $n = 3$  per group) against K562 (**f**), HL-60 (**g**), NALM6 (**h**), A1847 (**i**), MOLM-13 (**j**) and THP-1 (**k**). **l**, Schematic diagram of the measurement of serial killing cytotoxicity of iNK cells. **m**, Statistical analysis of the serial killing cytotoxicity of iNK cells and in same-donor expanded UCB-NK cells ( $n = 4$  per

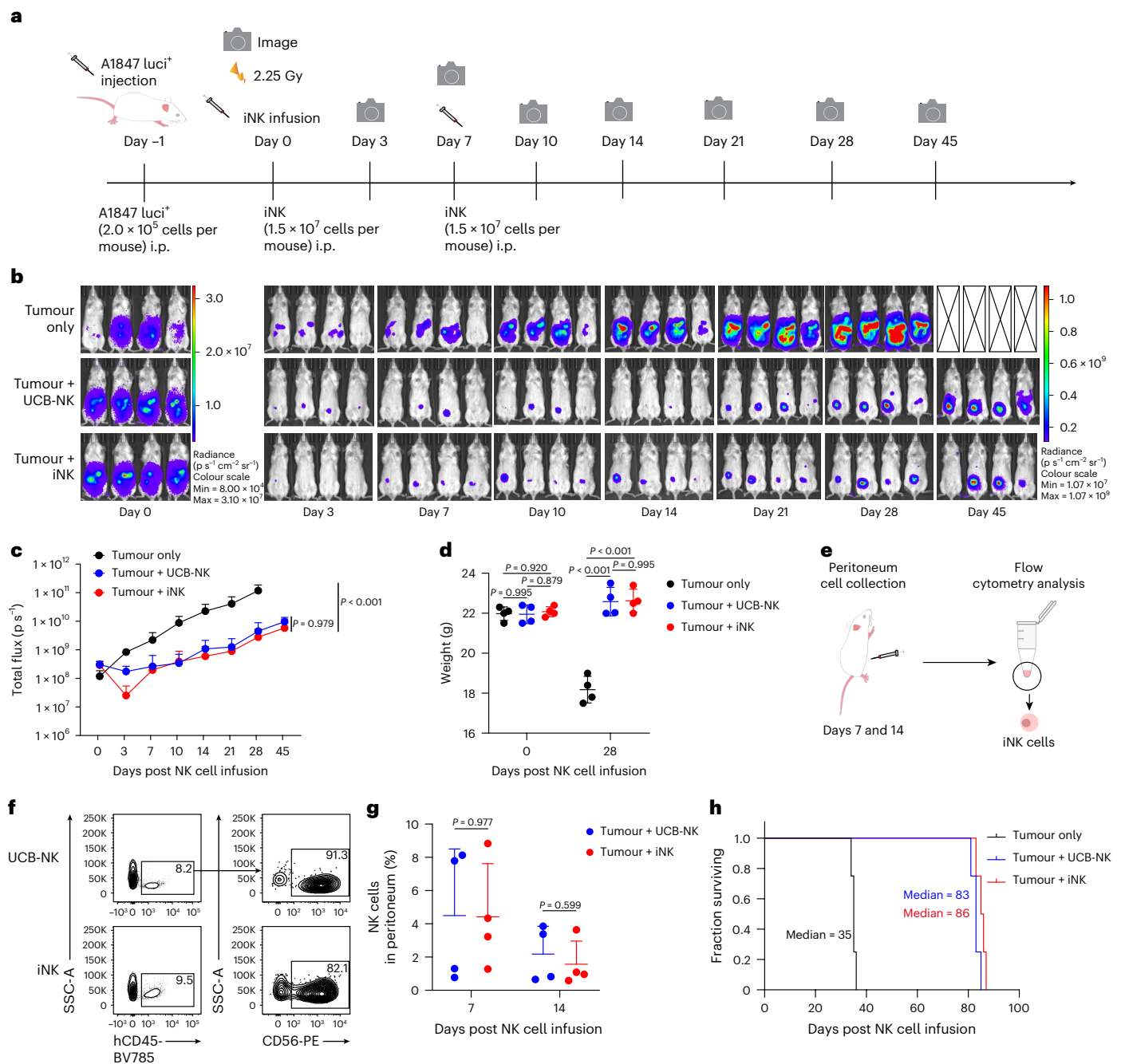
group). **n**, Representative flow cytometry histograms showing the expression profiles of NK cell activation receptors before (Unstimulated) and after (Round 3) the serial killing assay. **o**, Statistical analysis of mean fluorescence intensity (MFI) of activation receptors after the serial killing assay (Round 3) ( $n = 3$  per group). **p**, Representative flow cytometry histograms showing the expression profiles of NK cell inhibitory receptors before and after the serial killing assay. **q**, Statistical analysis of MFI of inhibitory receptors after the serial killing assay (Round 3) ( $n = 3$  per group). **r**, Representative flow cytometry histograms showing the expression profiles of NK cell exhaustion receptors before and after the serial killing assay. **s**, Statistical analysis of MFI of exhaustion receptors after the serial killing assay (Round 3) ( $n = 3$  per group). Data are presented as mean  $\pm$  s.d. of three technical repeats (**d,f–k,o,q,s**) or four technical repeats (**m**) from the same experimental unit, representative of three independent experiments. *P* values were calculated using unpaired two-sided *t*-test (**d,g–k,m,o,q,s**) or two-sided Mann–Whitney *U*-test (**d,f,j,o**). Exact *P* values are labelled.

cord-blood donor in the serial killing assay (Fig. 3m). Furthermore, we analysed the expression patterns of NK cell classical activation receptors (Nkp46, DNAM-1, 2B4 and NKG2D), inhibitory receptors (CD161 and CD328) and exhaustion receptors (TIGIT, PD-1 and TIM-3) before and after three rounds of tumour cell killing tests<sup>36–38</sup> (Fig. 3n–s). The mean fluorescence intensity (MFI) of DNAM-1 in iNK cells was higher than that in UCB-NK cells. However, the MFI of Nkp46, 2B4 and NKG2D

in iNK cells was not different from that of UCB-NK cells (Fig. 3n,o). The MFI of CD161 and CD328 in iNK cells was lower than that in UCB-NK cells (Fig. 3p,q). No significant differences were observed between iNK and UCB-NK cells in the upregulation of these exhaustion markers post tumour challenge (Fig. 3r,s). Collectively, CD34<sup>+</sup> HSPC-derived iNK cells express typical markers related to NK cell function and possess the ability to kill broad-spectrum tumours.







**Fig. 4 | iNK cells suppressed human tumour cell growth in xenograft animals.**

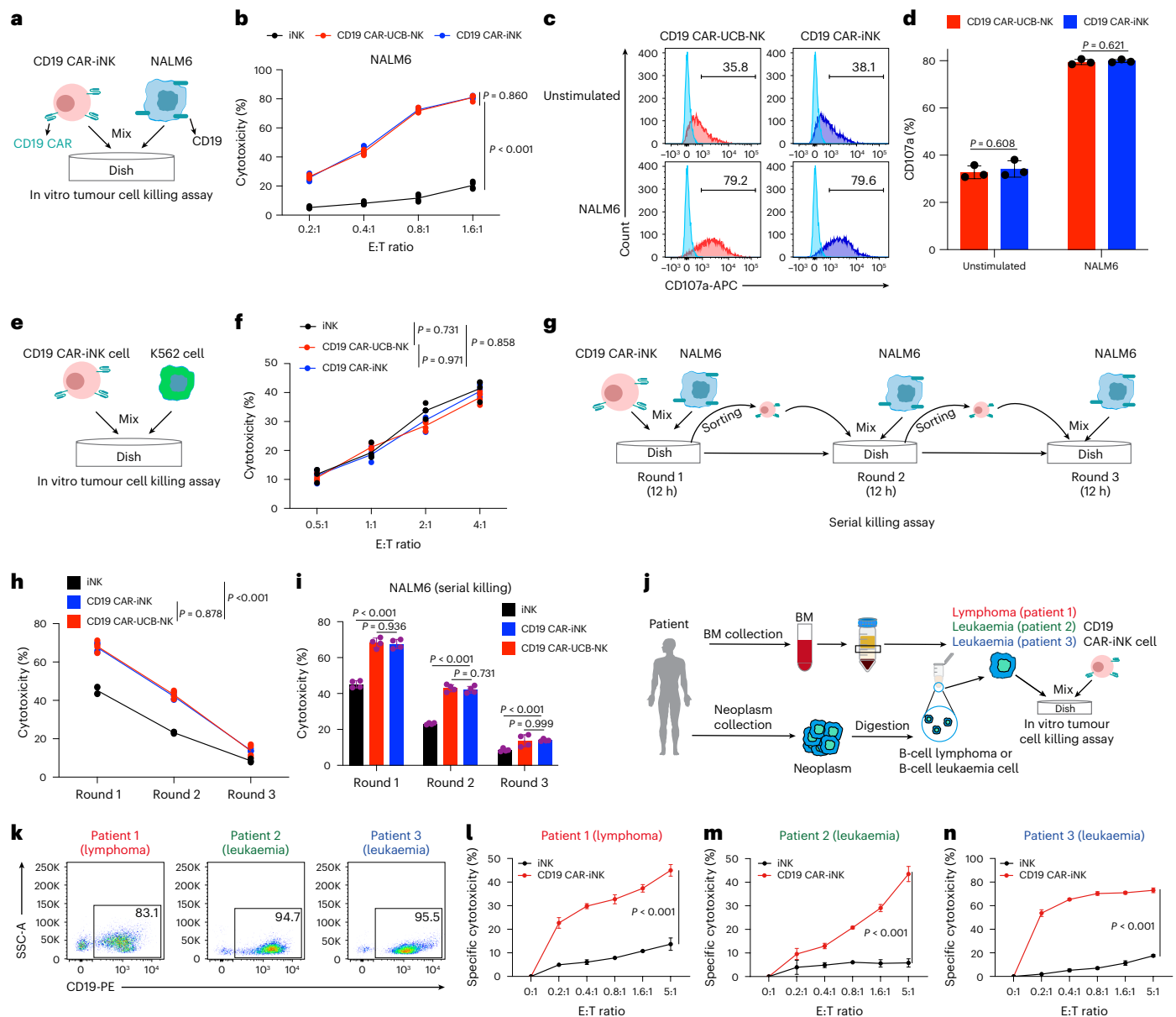
**a**, Schematic diagram of the evaluation of non-specific cytotoxicities of iNK cells in tumour-bearing mice. **b**, BLI analysis of the xenograft models ( $n = 4$  per group). **c**, Statistical analysis of total flux (photons per second,  $p \text{ s}^{-1}$ ) in xenograft models ( $n = 4$  per group). **d**, Statistical analysis of body weights of the xenograft models on day 28 after iNK cell injection ( $n = 4$  per group). **e**, Schematic diagram for analysis of the proportions of iNK or same-donor expanded UCB-NK cells (CD45<sup>+</sup>CD56<sup>+</sup>) in NK cell-treated xenograft models. **f**, Representative FACS plots showing the proportions of iNK cells or of same-donor expanded UCB-NK

cells (CD45<sup>+</sup>CD56<sup>+</sup>) in the peritoneum on day 7. **g**, Statistical analysis of the proportions of iNK cells or of same-donor expanded UCB-NK cells ( $n = 4$  per group). **h**, Kaplan-Meier survival curves for xenograft models ( $P < 0.001$ , log-rank test). Data are presented as mean  $\pm$  s.d. of four mice per group from the same experimental unit (**c**, **d**, **g**, **h**), representative of two independent experiments.  $P$  values were calculated using two-way analysis of variance (ANOVA) with Tukey's multiple comparisons test (**c**), one-way ANOVA with Tukey's multiple comparisons test (**d**) or unpaired two-sided  $t$ -test (**g**). Exact  $P$  values are labelled.

### CD34<sup>+</sup> HSPC-derived iNK cells suppressed tumour growth in A1847-tumour-bearing mice

To evaluate the in vivo therapeutic efficacy of HSPC-derived iNK cells, we established a human tumour cell line-derived xenograft model by intraperitoneal (i.p.) injection of luciferase-expressing A1847 cells (A1847-luciferase<sup>+</sup>,  $2.0 \times 10^5$  cells per mouse) into NCG mice on day -1. We infused iNK cells ( $1.5 \times 10^7$  cells per dose, i.p.) twice into

the tumour-bearing animals on days 0 and 7. In parallel, we used same-donor expanded UCB-NK cells as a treatment control. Weekly bioluminescence imaging (BLI) was performed to capture the dynamics of tumour burden (Fig. 4a). As expected, iNK cells effectively suppressed tumour growth in vivo, demonstrating tumour-killing efficiencies comparable to those of UCB-NK cells (Fig. 4b,c). In contrast, tumour-only animals exhibited progressive intensification of tumour



**Fig. 5 | CD19 CAR-iNK cells exhibited specific tumour-killing activities against B-cell lymphoma and leukaemia in vitro. a**, Schematic diagram of the evaluation of in vitro specific cytotoxicities of CD19 CAR-iNK cells. **b**, Statistical analysis of the specific cytotoxicities of CD19 CAR-iNK cells, iNK cells and same-donor-generated CD19 CAR-UCB-NK cells. **c**, Representative FACS plots showing the expression levels of CD107a of CD19 CAR-iNK cells and same-donor-generated CD19 CAR-UCB-NK cells after being stimulated with NALM6. **d**, Statistical analysis of the expression levels of the CD107a protein in **c** ( $n = 3$  per group). **e**, Schematic diagram of the evaluation of non-specific cytotoxicities of CD19 CAR-iNK cells. **f**, Statistical analysis of the non-specific cytotoxicities of CD19 CAR-iNK cells, iNK cells and same-donor-generated CD19 CAR-UCB-NK cells ( $n = 4$  per group). **g**, Schematic diagram of the evaluation of serial killing cytotoxicities of CD19 CAR-iNK cells. **h**, **i**, Statistical analysis of consecutive specific cytotoxicities of CD19 CAR-iNK cells ( $n = 4$  per group), showing the dynamic changes in cytotoxic activity among iNK, CD19 CAR-iNK and CD19 CAR-UCB-NK cells across the three rounds of killing assays (**h**) and the differences in cytotoxic activity among iNK, CD19 CAR-iNK and

CD19 CAR-UCB-NK cells at each round of the killing assay (**i**). Panels **h** and **i** show the same dataset using a line chart and a bar chart, respectively. **j**, Schematic diagram showing the specific cytotoxicities of CD19 CAR-iNK cells against CD19-expressing tumour cells isolated from patients with B-cell leukaemia or B-cell lymphoma. BM, bone marrow. **k**, Representative FACS plots showing the expression levels of CD19 protein in patient-derived B-cell lymphoma or leukaemia cells (gated from CD45<sup>+</sup>). **l–n**, Statistical analysis of the specific cytotoxicities of CD19 CAR-iNK cells against patient-derived B-cell lymphoma cells ( $n = 3$  per group) of patient 1 (**l**) or patient-derived B-cell leukaemia cells ( $n = 3$  per group) of patient 2 (**m**) and patient 3 (**n**). Data are presented as mean  $\pm$  s.d. of three technical repeats (**d**, **f**, **h**) or four technical repeats (**b**, **f**, **h**) from the same experimental unit, representative of three independent experiments.  $P$  values were calculated using two-way ANOVA with Tukey's multiple comparisons test (**b**, **f**, **h**) or Bonferroni post test (**l–n**), unpaired two-sided  $t$ -test (**d**), or one-way ANOVA with Tukey's multiple comparisons test or Tamhane T2 multiple comparisons test (**i**). Exact  $P$  values are labelled.

burden, evidenced by increased radiance and total flux (Fig. 4b,c). iNK and UCB-NK cell-treated animals maintained stable body weight for 28 days. However, the tumour-only group showed significant body loss (Fig. 4d). We further investigated the dynamics of UCB-NK cells

and iNK cells (hCD45<sup>+</sup>CD56<sup>+</sup>) in the peritoneum after cell infusion (Fig. 4e). We detected  $4.5 \pm 4.0\%$  ( $n = 4$ ) of UCB-NK cells or  $4.4 \pm 3.2\%$  ( $n = 4$ ) of iNK cells in total nuclear cells of peritoneal dropsy from treated mice on day 7 (Fig. 4f,g). CD45<sup>+</sup>CD56<sup>+</sup> cells in the peritoneum

decreased to much lower levels in UCB-NK cell-treated mice ( $2.2 \pm 1.7\%$ ,  $n = 4$ ) and iNK cell-treated mice ( $1.6 \pm 1.4\%$ ,  $n = 4$ ) on day 14 (Fig. 4g). However, the kinetics of UCB-NK cells and iNK cells exhibited similar patterns (Fig. 4g). In particular, both the iNK cells and the UCB-NK cells significantly prolonged the survival of treated tumour-bearing animals (tumour-only: 35 days; tumour + UCB-NK: 83 days; tumour + iNK: 86 days;  $P < 0.001$ ) (Fig. 4h). In conclusion, these results show that the CD34<sup>+</sup> HSPC-derived iNK cells suppress tumour cell growth and markedly extend the survival of A1847-tumour-bearing animals.

### CD19 CAR-iNK cells efficiently eliminated B-cell lymphoma and leukaemia tumour cells

We analysed the phenotypic profiles of classical NK cell activating receptors, inhibitory receptors and apoptosis-related ligands in CD19 CAR-iNK cells. The same-donor-prepared CD19 CAR-UCB-NK cells were used as the positive control. Flow cytometry analysis showed that the expression levels of these proteins were similar in CD19 CAR-iNK and CD19 CAR-UCB-NK cells (Extended Data Fig. 6d). To confirm the specific cytotoxicity of CD19 CAR-iNK cells, we performed in vitro tumour-killing assays by separately co-culturing CD19 CAR-iNK cells with CD19-positive NALM6 cells, primary tumour cells of CD19-positive human B-cell lymphoma and leukaemia. We first selected the NALM6 tumour cell line for the tumour-killing effect of CD19 CAR-iNK cells. Initially, NALM6 cells (as targets, T) were incubated with CD19 CAR-UCB-NK cells, iNK cells and CD19 CAR-iNK cells (effectors, E) separately at E:T = 0.2:1, 0.4:1, 0.8:1 and 1.6:1 for 4 h (Fig. 5a). As expected, CD19 CAR-iNK cells showed superior cytotoxicity against tumour targets than iNK cells. CD19 CAR-iNK cells showed specific cytotoxicity similar to that of CD19 CAR-UCB-NK cells (Fig. 5b). We then analysed the expression of CD107a in CD19 CAR-iNK cells and CD19 CAR-UCB-NK cells. Our result showed that CD19 CAR-iNK cells exhibited similar expression levels of CD107a as CD19 CAR-UCB-NK cells (Fig. 5c,d). Furthermore, we also evaluated the non-specific tumouricidal capacity of CD19 CAR-iNK cells using K562 tumour cells (Fig. 5e). Our results indeed demonstrated that these CD19 CAR-iNK cells retained non-specific cytotoxicity similar to that of CD19 CAR-UCB-NK and iNK cells (Fig. 5f). To assess the sustained cytotoxic activity of CD19 CAR-iNK cells, we performed serial tumour-killing assays with NALM6 tumour cells at an E:T ratio of 1:1 (Fig. 5g). Throughout three rounds, CD19 CAR-iNK cells maintained constant superior cytotoxicity compared with iNK cells. The cytotoxic activities of CD19 CAR-iNK cells and CD19 CAR-UCB-NK cells were not significantly different in the serial killing assay (Fig. 5h,i). Therefore, CD19 CAR-HSPC-derived CD19 CAR-iNK cells possess specific cytotoxicity against CD19-positive tumour cells and maintain the non-specific tumouricidal capacity of NK cells. Next, we tested the specific cytotoxicity of CD19 CAR-iNK cells against CD19-positive primary tumour cells from patients with B-cell lymphoma and B-cell leukaemia (Fig. 5j). Our results showed that CD19 CAR-iNK cells exhibited increased cytotoxicity against patient-derived B-cell lymphoma (patient 1) and B-cell leukaemia cells (Patients 2 and 3). However, iNK cells showed limited cytotoxicity against tumour cells from these three patients even at higher E:T ratios (Fig. 5k-n).

Collectively, CD19 CAR-iNK cells exhibit superior specific cytotoxicity against CD19-positive tumour cells and still possess serial killing capacity and maintain the non-specific cytotoxicity of NK cells.

### CD19 CAR-iNK cells suppressed tumour growth in NALM6 tumour-bearing mice

To evaluate the therapeutic efficacy in vivo of CD19 CAR-iNK cells, we established B-ALL xenograft animal models using NALM6 cells expressing luciferase (NALM6-luc<sup>+</sup>). On day -1, B-NDG hIL15 mice were injected intravenously (i.v.) with  $1 \times 10^5$  NALM6-luc<sup>+</sup> cells. Tumour-bearing mice were injected with control iNK cells or CD19 CAR-iNK cells ( $\sim 1.0 \times 10^7$  CD19 CAR-iNK cells per dose, two doses) through the tail veins. Tumour progression was monitored weekly using BLI (Fig. 6a). iNK cell treatment

alone did not suppress NALM6 cell growth in vivo, consistent with the observations in UCB-NK cell-treated NALM6 tumour-bearing animals<sup>27</sup>. As expected, CD19 CAR-iNK cells effectively suppressed tumour growth in vivo, demonstrating superior tumour-killing efficiencies compared with iNK cells (Fig. 6b,c). We further investigated the in vivo kinetics of iNK cells and CD19 CAR-iNK cells in tumour-bearing mice (Fig. 6d). We observed apparent human CD45<sup>+</sup>CD56<sup>+</sup> iNK cells that circulated in the peripheral blood of the animals treated with iNK cells ( $7.4 \pm 2.2\%$ ,  $n = 5$ ) and those treated with CD19 CAR-iNK cells ( $10.0 \pm 1.7\%$ ,  $n = 5$ ) on day 7 (Fig. 6e,f). However, circulating CD45<sup>+</sup>CD56<sup>+</sup> decreased to much lower levels in mice treated with iNK cells ( $1.2 \pm 0.8\%$ ,  $n = 5$ ) and mice treated with CD19 CAR-iNK cells ( $1.9 \pm 1.4\%$ ,  $n = 5$ ) on day 14 (Fig. 6f). In particular, the CD19 CAR-iNK cell therapy significantly extended the survival of NALM6 tumour-bearing mice (tumour-only: 25 days; tumour + iNK: 27 days; tumour + CD19 CAR-iNK: 49 days;  $P < 0.001$ ) (Fig. 6g). We further compared the in vivo anti-tumour efficacies between CD19 CAR-iNK cells and CD19 CAR-UCB-NK. We used revived (that is, thawed after cryopreservation, see next section) CD19 CAR-iNK cells and same-donor cord blood-generated CD19 CAR-UCB-NK cells to treat the NALM6 cell-bearing mice. As expected, CD19 CAR-iNK cells showed similar therapeutic efficacy as the CD19 CAR-UCB-NK cells (Extended Data Fig. 7a-f). Our data demonstrate that CD19 CAR-iNK cells can efficiently kill CD19-positive tumour cells in vivo and prolong the survival of tumour-bearing animals.

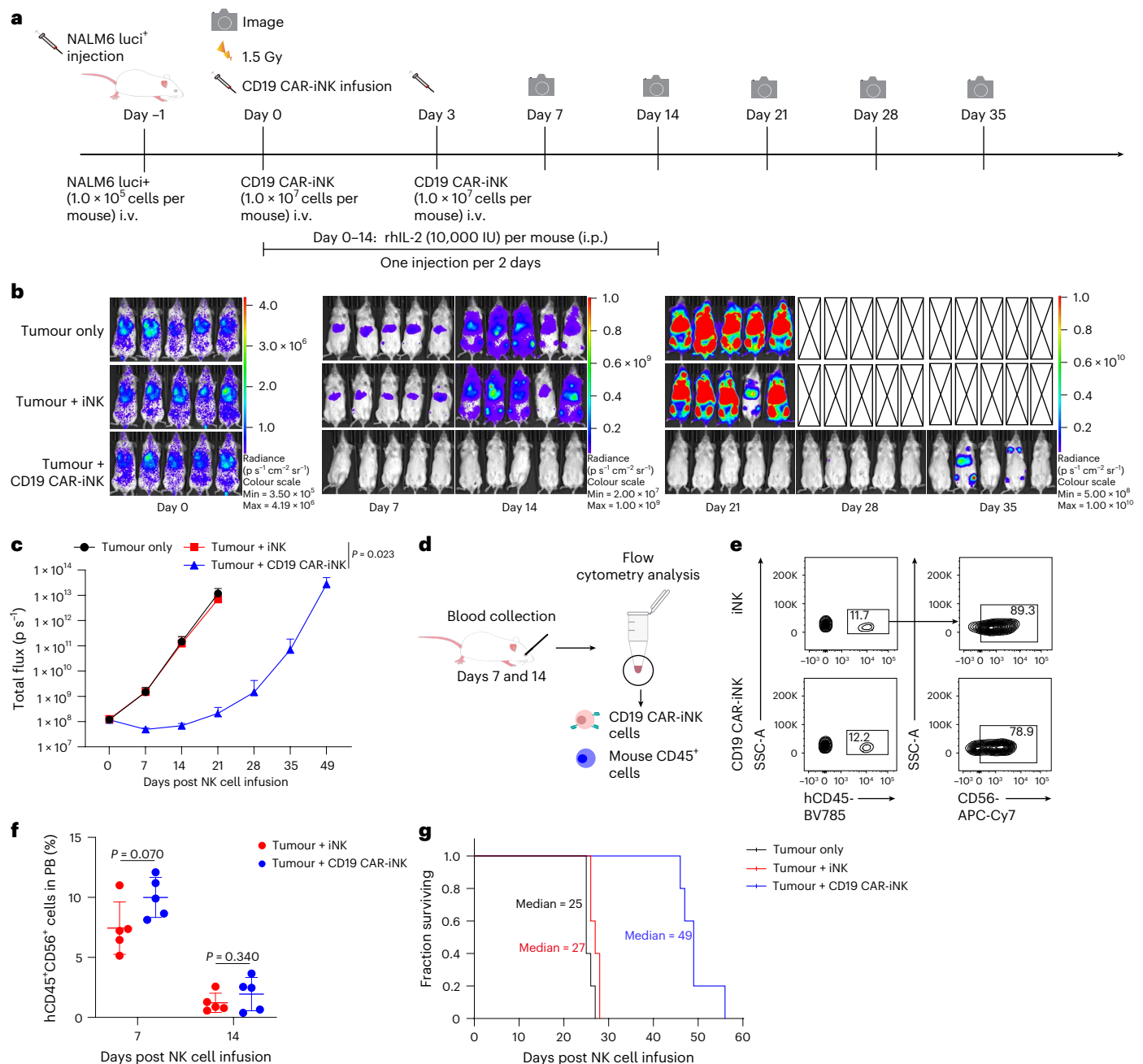
### Cryopreserved CD19 CAR-iNK cells retained tumour-killing efficacies in vitro and in vivo

To mimic potential 'off-the-shelf' products of CD19 CAR-iNK cells, we collected and cryopreserved CD19 CAR-iNK cells using commercial GMP-grade CryoStor CS10 cell-freezing medium<sup>39</sup>. After 6 months, cryopreserved cells were thawed and revived for recovery tests for 24, 48 and 72 h to assess dynamic variations in their viability, cell numbers and tumour-killing activities (Fig. 7a). After 72 h of in vitro revival, the viabilities of iNK cells reached  $87.8 \pm 1.1\%$  ( $n = 3$ ). The viabilities of CD19 CAR-iNK cells were  $90.0 \pm 1.1\%$  ( $n = 3$ ) (Fig. 7b,c). Furthermore, after 72 h of in vitro culture, the iNK and CD19 CAR-iNK cell counts were restored to  $89.2 \pm 2.8\%$  ( $n = 3$ ) and  $91.2 \pm 3.8\%$  ( $n = 3$ ) of pre-cryopreservation input counts, respectively (Fig. 7d,e). NALM6 tumour-killing assays showed that revived iNK cells showed weaker cytotoxicities than fresh iNK cells only at E:T ratios of 0.4:1 and 0.8:1 (Fig. 7f). Interestingly, the revived CD19 CAR-iNK cells exhibited cytotoxicities similar to those of fresh CD19 CAR-iNK cells (Fig. 7g).

Furthermore, we evaluated the in vivo tumour killing efficacy of cryopreserved CD19 CAR-iNK cells (Fig. 7h). As expected, thawed CD19 CAR-iNK cells without extended culture revival still retained enhanced anti-tumour activity over iNK cells in vivo (Fig. 7i,j). We also observed apparent human CD45<sup>+</sup>CD56<sup>+</sup> iNK cells circulating in the peripheral blood of the animals treated with iNK cells ( $11.4 \pm 2.8\%$ ,  $n = 4$ ) or CD19 CAR-iNK cells ( $12.7 \pm 2.6\%$ ,  $n = 4$ ) on day 7 (Fig. 7k,l). However, circulating CD45<sup>+</sup>CD56<sup>+</sup> decreased to much lower levels in mice treated with iNK cells ( $1.1 \pm 0.4\%$ ,  $n = 4$ ) and mice treated with CD19 CAR-iNK cells ( $1.7\% \pm 0.7\%$ ,  $n = 4$ ) on day 14 (Fig. 7l). In particular, thawed CD19 CAR-iNK cell therapy significantly extended the survival of NALM6 tumour-bearing mice (tumour-only: 24 days; tumour + iNK: 26 days; tumour + CD19 CAR-iNK: 43 days;  $P < 0.001$ ) (Fig. 7m).

To further investigate the tumour-killing efficacy of CD19 CAR-iNK cells against B-ALL patient-derived primary tumour cells, we constructed a B-ALL PDX model using the primary B-ALL cells from a patient carrying an FLT3-TKD mutation and an MLL-ENL fusion. The patient-derived primary tumour cells were from cryopreserved samples, the revival of which showed a high ratio of dying cells and led to an extremely low transduction rate of luciferase virus. We intravenously injected the revived primary B-ALL cells (5 million per mouse) into B-NDG mice to allow the tumour cells to proliferate in the body. We killed the mice and collected the fresh B-ALL cells from spleens at



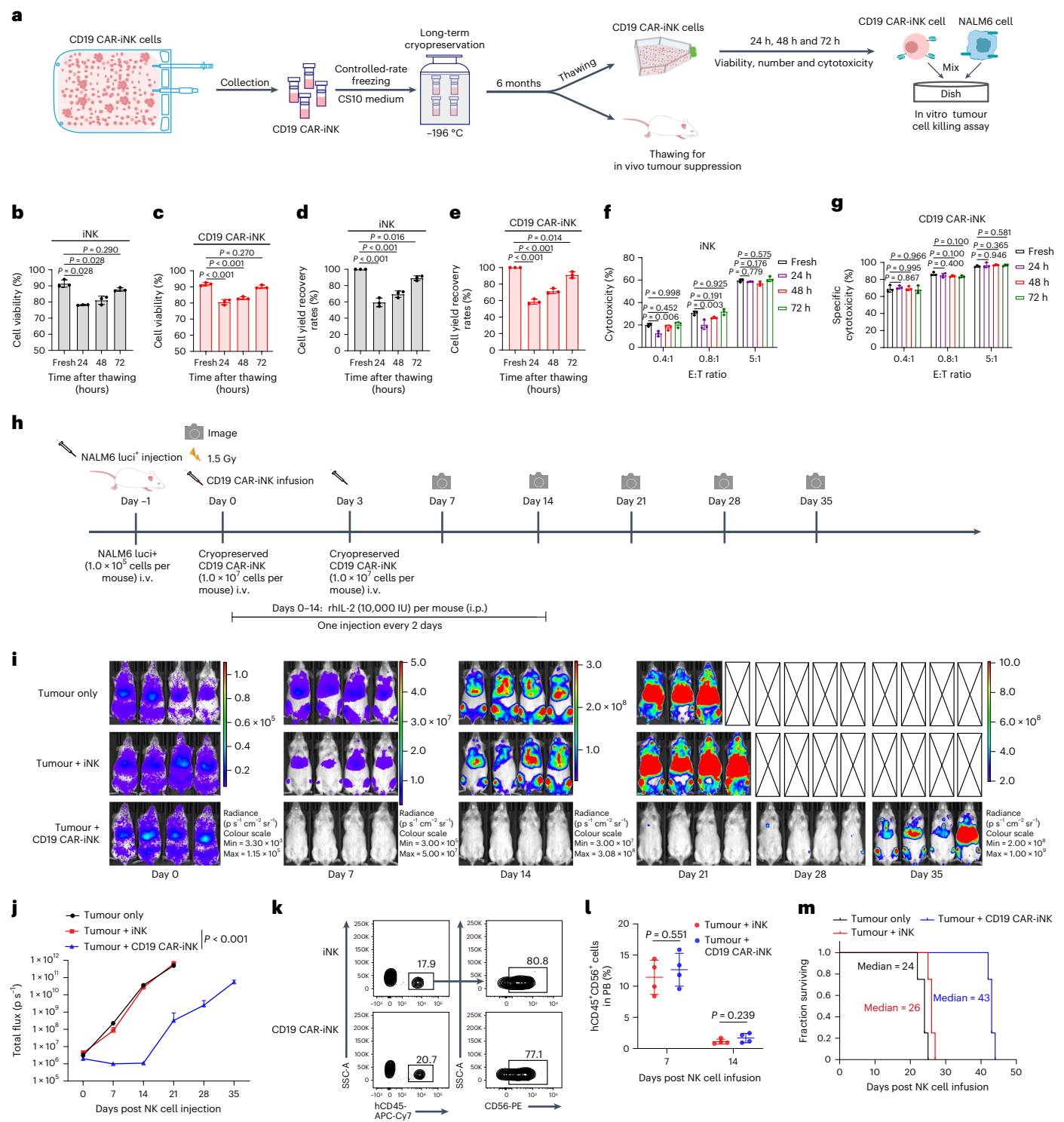


**Fig. 6 | CD19 CAR-iNK cells suppressed the growth of human B leukaemia cells in xenograft animals. a**, Schematic diagram of the evaluation of in vivo cytotoxicities of CD19 CAR-iNK cells. **b**, BLI analysis of the xenograft models ( $n = 5$  per group). **c**, Statistical analysis of total flux ( $p \text{ s}^{-1}$ ) in xenograft models ( $n = 5$  per group). **d**, Schematic diagram for analysis of the proportion of human CD45<sup>+</sup>CD56<sup>+</sup> cells in peripheral blood (PB). **e**, Representative FACS plots showing the proportion of human CD45<sup>+</sup>CD56<sup>+</sup> cells from PB in tumour-bearing mice on

day 7. **f**, Statistical analysis of the proportions of hCD45<sup>+</sup>CD56<sup>+</sup> NK cells in the peripheral blood of tumour-bearing mice on days 7 and 14 ( $n = 5$  per group). **g**, Kaplan-Meier survival curves for xenograft models ( $P < 0.001$ , log-rank test). Data are presented as mean  $\pm$  s.d. of five mice per group from the same experimental unit (**c**, **f**, **g**), representative of two independent experiments.  $P$  values were calculated using two-way ANOVA with Tukey's multiple comparisons test (**c**) or unpaired two-sided  $t$ -test (**f**). Exact  $P$  values are labelled.

6 weeks post injection for tumour-killing assay in vitro and for the luciferase virus transduction assay (Fig. 8a). We incubated the fresh B-ALL cells with CD19 CAR-iNK cells at indicated E:T ratios. The CD19 CAR-iNK cells significantly killed more tumour cells than the iNK cells at all E:T ratios (Fig. 8b). The B-ALL-killing abilities of CD19 CAR-iNK cells and CD19 CAR-UCB-NK cells showed no significant difference at all E:T ratios (Fig. 8b). To construct the luciferase-expressing B-ALL primary xenograft models, the proliferating tumour cells isolated from the inoculated animals were immediately infected with lentiviruses carrying the Luciferase-E2A-tdTomato expression cassette. At

72 h post infection, the luciferase-expressing B-ALL cells (B-ALL luciferase<sup>+</sup>) comprised 18.6% (Fig. 8a). We sorted the B-ALL luciferase<sup>+</sup> cells to construct PDX models (Fig. 8a). We intravenously injected the B-ALL luciferase<sup>+</sup> cells ( $2.0 \times 10^6$  cells per mouse) into B-NDG hIL15 mice on day -1. BLI was performed to determine the tumour burden of these mice on day 0. Mice with similar tumour burden were randomly divided into four groups: tumour-only, iNK, CD19 CAR-UCB-NK and CD19 CAR-iNK ( $n = 5$  per group). Then, the thawed iNK cells, CD19 CAR-UCB-NK cells and CD19 CAR-iNK cells ( $\sim 1.0 \times 10^7$  CD19 CAR<sup>+</sup> NK cells per mouse) were intravenously injected into the B-ALL luciferase<sup>+</sup> cell-bearing mice on days



**Fig. 7 | Cryopreserved CD19 CAR-iNK cells retained tumour-killing efficacies in vitro and in vivo. a**, Schematic diagram for the evaluation of specific cytotoxicities of the cryopreserved CD19 CAR-iNK cells in vitro and in vivo. **b,c**, Statistical analysis of the viabilities of iNK cells (**b**) and CD19 CAR-iNK cells (**c**) after thawing for 24 h, 48 h and 72 h. ( $n = 3$  per group). **d,e**, Statistical analysis of cell yield recovery rates of iNK (**d**) and CD19 CAR-iNK (**e**) cells after thawing for 24 h, 48 h and 72 h. ( $n = 3$  per group). **f,g**, Statistical analysis of the cytotoxicities of iNK cells (**f**) and CD19 CAR-iNK cells (**g**) against NALM6, after thawing for 24 h, 48 h and 72 h at the indicated E:T ratios ( $n = 3$  per group). **h**, Schematic diagram of the evaluation of specific cytotoxicities of the cryopreserved CD19 CAR-iNK cells in vivo. **i**, BLI analysis of the xenograft models ( $n = 4$  per group). **j**, Statistical analysis of total flux in xenograft models ( $n = 4$  per group). **k**, Representative

FACS plots showing the proportions of iNK and CD19 CAR-iNK cells (hCD45<sup>+</sup>CD56<sup>+</sup>) in peripheral blood on day 7. **l**, Statistical analysis of the proportions of iNK cells and CD19 CAR-iNK cells (hCD45<sup>+</sup>CD56<sup>+</sup>) in peripheral blood on days 7 and 14 ( $n = 4$  per group). **m**, Kaplan–Meier survival curves for xenograft models ( $P < 0.001$ , log-rank test). Data are presented as mean  $\pm$  s.d. of three independent biological replicates (**b–e**) or three technical repeats from the same experimental unit (**f,g**) representative of three independent experiments, or 4 mice per group from the same experimental unit (**j,l,m**) representative of 2 independent experiments.  $P$  values were calculated using one-way ANOVA with Dunnett T3 multiple comparisons test (**b**) or Dunnett’s multiple comparisons test (**c–g**), two-sided Mann–Whitney  $U$ -test (**g**), two-way ANOVA with Tukey’s multiple comparisons test (**j**), or unpaired two-sided  $t$ -test (**l**). Exact  $P$  values are labelled.

0 and 3. BLI was performed and B-ALL cells (human CD45<sup>+</sup>CD19<sup>+</sup>) in PB were analysed every 7 days (Fig. 8c). The tumours of the tumour-only and the iNK groups proliferated rapidly and preferentially grew in spleens (Fig. 8d–f). Total flux values were much lower in CD19 CAR-iNK cell-treated mice, indicating that CD19 CAR-iNK cells significantly suppressed B-ALL tumour growth (Fig. 8f). Moreover, the total flux values showed no significant difference between CD19 CAR-iNK-treated mice and CD19 CAR-UCB-NK-treated mice (Fig. 8d–f). Similar to the rapid tumour-burden development, the percentages of B-ALL luciferase<sup>+</sup> cells in the PB of mice in the tumour-only group and the iNK group were also sharply increased (Fig. 8g). The median survival of mice in the tumour-only group and the iNK group were 28 days and 29 days, respectively. The median survival of mice in the CD19 CAR-iNK group and the CD19 CAR-UCB-NK group were 43 days and 42 days, respectively (Fig. 8h).

In summary, our data demonstrate that CD19 CAR-iNK cells maintain anti-tumour activity both in vitro and in vivo.

## Discussion

In this study, we develop an efficient three-step strategy that can generate millions of iNK cells and CD19 CAR-iNK cells from a single umbilical cord blood CD34<sup>+</sup> HSPC. The generating efficiencies of iNK cells and CD19 CAR-iNK cells are 6,918–20,224-fold higher than those of traditional methods<sup>10</sup>. Interestingly, our method reduces the engineering cost of CD19 CAR-iNK cells derived from CD34<sup>+</sup> HSPC and CD19 CAR-iNK cells possess ideal tumouricidal activities against human tumours. Our study provides insight into the use of CD34<sup>+</sup> HSPCs as cell sources to generate CAR-NK cells and expand their accessibility and affordability for patients.

We selected an SFG-based retroviral vector<sup>18,19</sup> that has been used in multiple clinical trials for CD19 CAR-NK cells<sup>8,9</sup> and CAR-T cells<sup>40,41</sup>. Our CD19 CAR-iNK cells showed CD19 CAR positivity rates ranging from 58.5% to 64.4%, comparable to the positivity rates of CD19 CAR-UCB-NK cells obtained by engineering mature UCB-NK cells (47.8%–87.4%, median = 66.6%)<sup>42</sup>. However, the CD19 CAR retroviral vector copy number ( $4.6 \pm 0.1$  per CAR<sup>+</sup> cell) in these CD19 CAR-iNK cells approaches the FDA-recommended upper limit (VCN < 5 per transduced cell). We further reduced the initial transduction rates to keep a lower VCN number and implemented a strategy of enrichment for CD19 CAR-HSPCs, which can ensure the eventual high CD19 CAR-positive rates in iNK cells. Transduction of CAR into CD34<sup>+</sup> HSPCs neither alters the differentiation efficiencies of the generation of CAR-iNK cells nor results in silencing of CAR expression in derived iNK cells. Moreover, all the CD19 CAR<sup>+</sup>CD34<sup>+</sup>, CD19 CAR<sup>+</sup>CD34<sup>+</sup> and CD19 CAR<sup>+</sup>CD34<sup>+</sup> populations on day 14 can output CAR-iNK cells with differential efficiencies. CD19 CAR<sup>+</sup>CD34<sup>+</sup> cells on day 14 possess the strongest potential for generating CAR-iNK cells. To increase yields of iNK cells and CAR-iNK cells, we directly use the bulk cells on day 14 for CAR-iNK cell induction.

Furthermore, in mouse models with NALM6 xenograft and patient-derived B-ALL xenograft, CD19 CAR-iNK cells showed specific killing activity similar to that of CD19 CAR-UCB-NK cells. Both CD19 CAR-iNK cells and CD19 CAR-UCB-NK cells showed superior specific killing activity compared with unmodified iNK cells. By administering  $1 \times 10^7$  CD19 CAR-iNK cells twice, we achieved similar suppression effects on tumour growth, confirming the therapeutic potential and applicability of CD19 CAR-iNK cells in anti-tumour therapy. However,

unlike long-term therapeutic efficacies observed with a single-dose CD19 CAR-T treatment in animal models and in certain patients, two doses of CD19 CAR-iNK cell treatment still lack persistent therapeutic efficacy in tumour-bearing animals, indicating that multiple and high doses of CAR-iNK cell therapy are critical for persistent suppression of tumours. However, our method produces large-scale iNK and CAR-iNK cells from CD34<sup>+</sup> HSPCs to prospectively treat human cancers.

Over decades, the AFT024 cell line has been a feeder cell priority for the expansion of human CD34<sup>+</sup> HSPCs, which ideally maintains the stemness and curbs the differentiation of human long-term haematopoietic stem cells (HSCs)<sup>20–22</sup>. In our approach, AFT024 cells further expanded CD34<sup>+</sup> HSPCs without losing their differentiation potential from the NK lineage. The 14-day expansion based on AFT024 feeder cells in the presence of HSC culture medium<sup>23</sup> significantly increases the iNK and CAR-iNK cell yields by >160 times, indicating that the potential of the NK lineage is preserved primarily in expanded CD34<sup>+</sup> HSPCs. Our method reliably produces large-scale homogeneous iNK cells and CAR-iNK cells from a single donor umbilical cord blood unit of CD34<sup>+</sup> HSPCs, which prospectively provides for 760–83,000 doses ( $10^9$ – $10^{10}$  cells per dose)<sup>8,9</sup> to treat tumour patients. Our result shows that the thawed CD19 CAR-iNK cells retain anti-tumour efficacy, providing obvious leverages for long-term safety inspections of CAR-NK products and comprehensive clinical applications. Thus, in clinical settings, the tumorigenic risks of CAR-iNK cells can be well evaluated in animal models before large-scale clinical applications, as autogenous CAR-T-cell therapies reportedly show a few cases of CAR-T-derived secondary T-cell tumours<sup>43</sup>. Our method shows that engineering CAR at the CD34<sup>+</sup> HSPC stage barely harms iNK induction efficiencies. Interestingly, the CD19 CAR expression rates in our method maintain consistently high levels (58.5%–64.4%), indicating that there is no obvious silencing of CAR expression during the entire three-step process. We propose that our method can reduce the manufacturing expense of CAR-iNK cells by significantly lowering the cost of CAR engineering at the CD34<sup>+</sup> HSPC stage, which might promote the accessibility of this type of cell therapy.

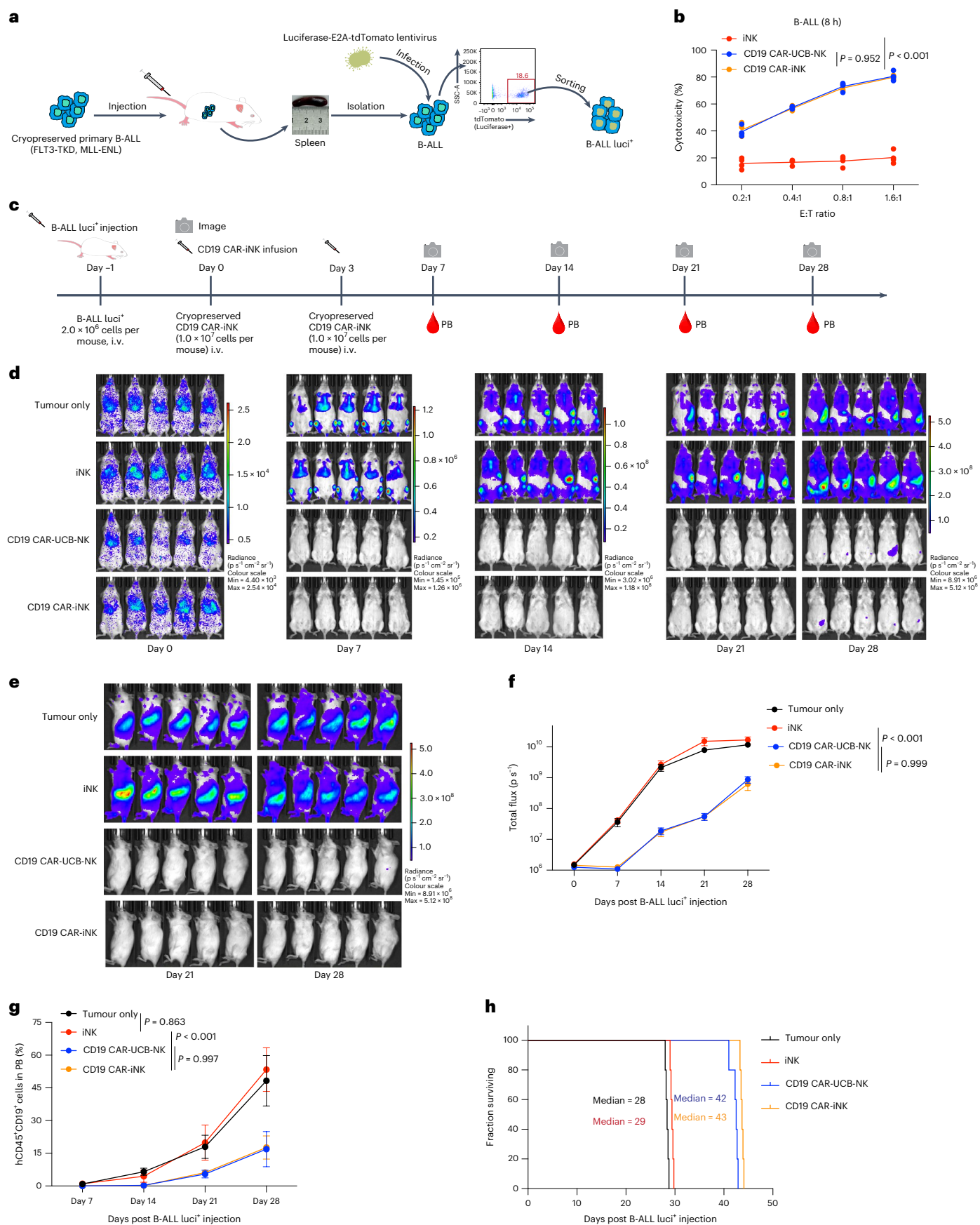
In this study, we used mouse stromal cells AFT024 and OP9 to extremely elevate the generating efficiency and reduce the CAR engineering cost of CAR-iNK cells. However, the use of murine-derived stromal cells would make the translation of this approach to the clinic challenging. AFT024 are irradiated at a dose of 20 Gy before use, which reduces potential safety risks. As for the use of the OP9 cell line for iNK cell induction from pluripotent stem cells (PSCs), a recent clinical trial (JK500, [NCT05519384](https://clinicaltrials.gov/ct2/show/study?term=JK500&rank=1)) using the iNK cells for treating acute myeloid leukemia patients primarily proved its safety. Comprehensive safety and toxicity tests were completed for JK500 in line with current recommendations from the Center for Drug Evaluation (CDE) under China's National Medical Products Administration (NMPA). To move forward to a potential clinical trial of CAR-iNK cells prepared by our method, we will also perform these tests on CD19 CAR-iNK cells, including pathogen testing (fungi, bacteria, viruses and mycoplasma), karyotype analysis, purity assessment of CAR-iNK cells (excluding residual feeder cells and CAR-HSPCs), short tandem repeat profiling, tumorigenicity evaluation, cytotoxicity evaluation, pharmacokinetic monitoring of CAR-iNK cells in vivo, and phenotypic and functional characterization of CAR-iNK cells.

However, it is necessary to develop alternative ways of replacing the existing feeder systems to facilitate clinical translation and drug

**Fig. 8 | CD19 CAR-iNK cells suppressed the growth of primary human B-ALL cells in PDX models.** **a**, Schematic diagram for the construction of luciferase-expressing patient-derived primary B-ALL cells (B-ALL luciferase<sup>+</sup>). **b**, Statistical analysis of the specific cytotoxicities of CD19 CAR-iNK cells, iNK cells and same-donor-generated CD19 CAR-UCB-NK cells against patient-derived primary B-ALL cells. **c**, Schematic diagram of the evaluation of cytotoxicities of CD19 CAR-iNK cells in vivo. **d,e**, BLI analysis of the PDX models (ventral (**d**) and left (**e**);  $n = 5$  per group). **f**, Statistical analysis of total flux of the PDX models in **d** ( $n = 5$  per group).

**g**, Statistical analysis of the proportions of B-ALL-luciferase<sup>+</sup> cells (CD45<sup>+</sup>CD19<sup>+</sup>) in the peripheral blood of the PDX models ( $n = 5$  per group). **h**, Kaplan–Meier survival curves for xenograft models ( $P < 0.001$ , log-rank test). Data are presented as mean  $\pm$  s.d. of four technical repeats from the same experimental unit (**b**) representative of three independent experiments, or five mice per group from the same experimental unit (**f–h**) representative of two independent experiments.  $P$  values were calculated using two-way ANOVA with Tukey's multiple comparisons test (**b,f,g**). Exact  $P$  values are labelled.





development. We propose two strategies to replace these feeder cells. The first approach involves using humanized feeder cells to replace murine AFT024 and OP9, which might not compromise the inducing efficiency and functionality of derived iNK and CAR-iNK cells. Complying with related national law and ethics guidelines, it is permissible to use discarded fetal tissue cells for developing immortalized human stromal feeder cells, employing methods used for developing immortalized AFT024 and OP9 lines<sup>14,44–47</sup>. Humanized feeder cells derived from bone marrow stromal cells should also be engineered to knock out *CSF1* (ref. 45) to prevent myeloid lineage differentiation and promote lymphoid differentiation via IL-7 signalling<sup>47,48</sup>. However, even if humanized feeder cells could successfully replace OP9 and AFT024 in our induction system, it is critical to inactivate these feeder cells, such as by irradiation, to ensure the safety of CD34<sup>+</sup> HSPC-derived iNK or CAR-iNK cell products in clinical applications. The second approach is to explore feeder-free conditions with cytokines, compounds and other biomolecules in combination with engineered cell-free material substitutes. This requires identifying key proteins or other molecules secreted by AFT024 and OP9 that promote HSC proliferation and NK-lineage lymphoid differentiation. For example, a recent study identified that AFT024 cells express delta-like/preadipocyte factor-1 (DLK1), which contains EGF-like repeats and supports HSPC stemness and proliferation in Dexter-type co-cultures<sup>49</sup>. DLK1 could therefore be explored in CD34<sup>+</sup> HSPC culture systems to improve expansion outcomes. OP9 cells, due to the lack of macrophage colony-stimulating factor, naturally inhibit myeloid differentiation and favour lymphoid lineage commitment<sup>47</sup>. Small molecules that block myeloid pathways could be used to enhance NK lineage specification during CD34<sup>+</sup> HSPC induction. In addition, proteins and extracellular matrix (ECM) components secreted by feeder cells are known to play important roles in HSC maintenance, proliferation and differentiation<sup>50</sup>. EGF-stimulated OP9 or *v-erb-BB2*-transduced OP9 cells, in combination with mSFO2 medium, have shown improved support for B lymphoid differentiation and enhanced HSPC function<sup>51</sup>. This suggests the potential of identifying active proteins from EGF-stimulated OP9 or *v-erb-B2*-transduced OP9 cells to be used with NK differentiation media to guide NK lineage development. One study also reported that 13 proteins in OP9 cell secretions and extracts contribute to haematopoietic development via the Nrf2/Nfe2l2 pathway<sup>52</sup>. Given that engineered niches can maintain HSC characteristics<sup>53</sup>, screening secreted factors or ECM components from AFT024 and OP9 and combining them with cell-free biomaterials to build artificial niches represent a promising direction for feeder-free systems. Furthermore, lymphotoxin- $\alpha$  (LT $\alpha$ ) and LT $\beta$ R, expressed by bone marrow stromal cells, have been shown to promote differentiation of HSCs into NK cells<sup>54</sup>, suggesting the potential to use small-molecule enhancers of the lymphotoxin pathway to guide NK progenitor development<sup>55</sup>. In the long term, engineered cell-free material substitutes replacing feeder cells would be ideal for addressing translational safety concerns if the high generating efficiency of iNK cells and low cost achieved via the use of OP9 and AFT024 cells were not compromised.

CD34<sup>+</sup> HSPCs as a cell source have been widely used in clinical applications. Since CD34<sup>+</sup> HSPCs do not undergo reprogramming, CD34<sup>+</sup> HSPC-derived iNK cells and CAR-iNK cells pose minimal tumourigenic risk. CD34<sup>+</sup> HSPC-derived iNK cells and CAR-iNK cells have lower immunogenicity, making them more suitable for allogeneic transplantation. HSPCs from UCB have limited self-renewal capability. However, PSCs possess indefinite self-renewal capacity, which allows for the generation of an unlimited and replenishable NK cell supply. iPSCs, in particular, offer patient-specific or allogeneic off-the-shelf options with minimal donor-to-donor variability. However, iPSC-derived cells carry a risk of residual undifferentiated cells, which could lead to teratoma formation. Allogeneic iPSC-derived NK cells may trigger immune rejection unless engineered for immune evasion. iPSC-based NK cell production involves a higher initial cost than

CD34<sup>+</sup> HSPC-derived NK cell production. Considering that our method can produce  $8.3 \times 10^7 \pm 0.7 \times 10^7$  iNK cells and  $3.2 \times 10^7 \pm 0.2 \times 10^7$  CAR-iNK cells from single CD34<sup>+</sup> HSPCs, the manufacturing costs of CD34<sup>+</sup> HSPC-derived iNK and CAR-iNK cells are lower than the costs of PSC-derived iNK cells and CAR-iNK cells, partially due to the low induction efficiency of iNK cells and CAR-iNK cells from PSCs (1,000 iNK cells from a single PSC<sup>17</sup>). Of note, genetic modification of PSCs occurs at the pluripotent stage, allowing for precise and stable engineering. iPSC-based platforms enable the selection of single clones with the desired edits, reducing batch-to-batch variability. Genetic modifications in CD34<sup>+</sup> HSPCs occur before differentiation into NK cells but are less efficient than in PSCs.

In conclusion, we have developed a comprehensive technique for efficiently generating massive CD34<sup>+</sup> HSPC-derived iNK cells and CAR-iNK cells, with potential for trillion-scale yields and lower cost of CAR engineering from a single donor umbilical cord blood unit of CD34<sup>+</sup> HSPCs. Our study provides insight into the use of CD34<sup>+</sup> HSPCs as cell sources to generate CAR-NK cells and for future expansion of their accessibility and affordability for patients.

## Methods

### Ethics statement

NCG mice (NOD/ShiLtJGpt-*Prkdc*<sup>em26Cd52</sup>*Il2rg*<sup>em26Cd22</sup>/Gpt, Strain T001475, GemPharmatech), B-NDG (NOD.CB17-*Prkdc*<sup>scid</sup>*Il2rg*<sup>tm1Bcgen</sup>/Bcgen, Biocytogen, 110586) and B-NDG hIL15 (NOD.CB17-*Prkdc*<sup>scid</sup>*Il2rg*<sup>tm1</sup>*IL15*<sup>tm1(IL15)</sup>/Bcgen background, Biocytogen, 110600) mice were housed in SPF-grade animal facility at the Guangzhou Institutes of Biomedicine and Health, Chinese Academy of Sciences, and SPF-grade animal facility at the Institute of Zoology, Chinese Academy of Sciences. All animal-related procedures in this study received approval from the Institutional Animal Care and Use Committees (IACUC) of the Guangzhou Institutes of Biomedicine and Health, and the Institute of Zoology, Chinese Academy of Sciences. NK cell anti-tumour activity assessments in animals received approval from the Biomedical Research Ethics Committees of the Guangzhou Institutes of Biomedicine and Health, Chinese Academy of Sciences, and the IACUC of the Institute of Zoology, Chinese Academy of Sciences. Patient samples were used according to the provisions of the Declaration of Helsinki. All patient samples were collected with signatures of previous consent from the patient, and reviewed and approved by the ethics committee of the Jinan University First Affiliated Hospital or the Ethics Committee of the Institute of Hematology, Blood Diseases Hospital, CAMS and PUMC. This informed consent included allowing investigators to publish data arising from the tissues they obtained.

### Cell culture

The Guangdong Umbilical Cord Blood Bank (Guangzhou, China) provided umbilical cord blood samples. UCB-NK cells were cultured in KBM581 medium (Corning, 88-581-CM) supplemented with rhIL-2 (recombinant human interleukin-2, 200 IU ml<sup>-1</sup>, Miltenyi, 130-097-743) and SGR-SM medium (1%, DAKWE, 6122011). OP9 was cultured in  $\alpha$ -MEM medium (Gibco, 12571063) with 20% fetal bovine serum (FBS) (Ausbian, WS500T). K562 (ATCC, CCL-243), HL-60 (ATCC, CCL-240), THP-1 (ATCC, TIB-202), NALM6-luc<sup>+</sup> (kindly provided by Prof. Min Wang of the Leukemia Centre, Institute of Hematology and Blood Diseases Hospital, Chinese Academy of Medical Sciences, Tianjin, China), MOLM-13 (kindly provided by Prof. Hui Cheng of the Leukemia Centre, Institute of Hematology and Blood Diseases Hospital) and A1847-luc<sup>+</sup> (Honsun Biological) were cultured in RPMI 1640 medium (Gibco, C11875500BT) supplemented with 10% FBS. AFT024 (ATCC, SCRC-1007) was cultured in Dulbecco's modified Eagle medium (DMEM) (Gibco, C11965500BT) with 10% FBS, 55  $\mu$ M  $\beta$ -mercaptoethanol (Sigma-Aldrich, M3148) and 1 mM GlutaMAX (Gibco, 35050061). 293T (ATCC, CRL-3216) and Hela (Pricella, CL-0101) cells were cultured in DMEM with 10% FBS.

### CD19 CAR retrovirus and Luciferase-tdTomato lentivirus packaging

For the CD19 CAR retrovirus package, the CD19 CAR cassette of CAR-CD8 $\alpha$  Hinge-CD8 $\alpha$  TM-CD3 $\zeta$ , which was constructed in a previous publication<sup>27</sup>, was cloned into the SFG vector backbone (22493, Addgene)<sup>56</sup> to obtain SFG-CD19 CAR. Retroviral particles were packaged by 293T cells, which were transfected with SFG-CD19 CAR, a helper plasmid for the GAG and Pol proteins of the murine leukaemia virus (14887, Addgene), and an envelope plasmid with the RD114 gene<sup>57</sup> using polyethylenimine. CD19 CAR retrovirus supernatants were collected at 48 and 72 h after transfection. For the Luciferase-tdTomato lentivirus package, a second-generation packaging plasmid was used for producing viral particles<sup>58</sup>. Briefly, pRRSIN-Luciferase-E2A-tdTomato vectors, PSPAX2 vectors and pMD2.G vectors were co-transfected into 293T cells using polyethylenimine. Luciferase-tdTomato lentivirus supernatants were collected at 48 and 72 h after transfection. All virus supernatants were concentrated using Amicon Ultra-15 centrifugal filters (Millipore, UFC900324). The CD19 CAR retrovirus titre was determined using HeLa cells. The Luciferase-tdTomato lentivirus titre was determined using 293T cells.

### Human CD34<sup>+</sup> HSPC enrichment

Umbilical cord blood mononuclear cells were isolated by density gradient centrifugation (STEMCELL Technologies, 07851), and CD34<sup>+</sup> HSPCs were selected using immunomagnetic beads (Miltenyi Biotec, 130046702). Isolated CD34<sup>+</sup> HSPCs were cryopreserved or directly used for HSPC expansion.

### Generation of CD19 CAR-HSPCs

Human CD34<sup>+</sup> HSPCs were stimulated in a medium composed of Iscove's modified Dulbecco's medium (Thermo Fisher, 31980030) supplemented with 20% BIT 9500 serum substitute (STEMCELL Technologies, 09500), 0.1 mmol l<sup>-1</sup>  $\beta$ -mercaptoethanol (Sigma-Aldrich, M3148), 50 ng ml<sup>-1</sup> SCF protein (PeproTech, 300-07), 50 ng ml<sup>-1</sup> FLT3-L (PeproTech, 300-19), 10 ng ml<sup>-1</sup> IL-3 (PeproTech, 200-03), 10 ng ml<sup>-1</sup> TPO (PeproTech, 300-18), 10 ng ml<sup>-1</sup> of granulocyte stimulating factor (G-CSF) (PeproTech, 300-23) and 10 ng ml<sup>-1</sup> of IL-6 (PeproTech, 200-06) for 48 h (refs. 59,60). On day 3, activated CD34<sup>+</sup> HSPCs were transduced with CD19 CAR retroviral vector (MOI = 10), following the Vectofusin-1 transduction protocol (Miltenyi Biotec, 130-111-163)<sup>61</sup>. The transduced CD34<sup>+</sup> HSPCs were immediately collected for the CD19 CAR-HSPC expansion step.

### Generation of iNK cells and CD19 CAR-iNK cells with high yields and purities of umbilical cord blood CD34<sup>+</sup> HSPCs

iNK cells and CD19 CAR-iNK cells were generated using a three-step culture method. In detail, we attempted to expand  $1 \times 10^6$  CD34<sup>+</sup> HSPCs or CD19 CAR-HSPCs at step I. For the expansion of CD34<sup>+</sup> HSPCs, on day -2,  $2 \times 10^6$  AFT024 cells were initially seeded in 20 wells of a 24-well plate ( $1 \times 10^5$  cells per well) and irradiated on day -1 (20 Gy, Rad Source RS2000). On day 0,  $1 \times 10^6$  freshly isolated CD34<sup>+</sup> HSPCs were evenly transferred to 20 wells ( $5 \times 10^5$  cells per well) and co-cultured with irradiated AFT024 cells. The composition of CD34<sup>+</sup> HSPC expansion medium was previously reported<sup>23</sup>, including the following reagents: StemSpan SFEMII (STEMCELL Technologies, 09655), 1% penicillin-streptomycin (Gibco, 15140122), 50 nM UMI71 (MCE, HY-12878), 20 ng ml<sup>-1</sup> TPO (PeproTech, 300-18), 50 ng ml<sup>-1</sup> SCF (PeproTech, 300-07) and 50 ng ml<sup>-1</sup> Flt3L (PeproTech, 300-19). For the expansion of CD19 CAR-HSPCs, AFT024 cells were seeded on day -1 and irradiated on day 0. On day 2.5, all cells (starting from  $1 \times 10^6$  freshly isolated CD34<sup>+</sup> HSPCs) were equally transferred to 20 wells and co-cultured with irradiated AFT024 cells. Half the culture medium was replaced with fresh medium containing additives (2 $\times$ ) every 2 days. To prepare for the second-round expansion,  $6 \times 10^7$  AFT024 cells were evenly seeded into six T225 flasks ( $1 \times 10^7$  cells per flask) on day 5 and irradiated on day 6 (20 Gy). On day

7, the expanded CD34<sup>+</sup> HSPCs and CD19 CAR-HSPCs derived from the first-round expansion were collected and equally transferred to six T225 flasks with freshly irradiated AFT024 feeder cells. The CD34<sup>+</sup> HSPCs and CD19 CAR-HSPCs then underwent the second-round expansion for another 7 days. On day 14, expanded CD34<sup>+</sup> cells were cryopreserved as off-the-shelf expanded CD34<sup>+</sup> HSPCs for future iNK and CAR-iNK manufacturing or freshly used for the generation of iNK cells and CD19 CAR-iNK cells.

At step II, the expanded CD34<sup>+</sup> HSPCs and CD19 CAR-HSPCs collected from step I were assembled into organoids for the specified differentiation of the NK lineage. In step III, we prepared 50 organoid aggregates to produce the required CD45<sup>+</sup> cells as one input unit for a bag-based culture system. We made an organoid aggregate drop by mixing  $1 \times 10^4$  expanded CD34<sup>+</sup> HSPCs or CD19 CAR-HSPCs with  $5 \times 10^5$  OP9 cells (unirradiated). These organoids were cultured on 0.4- $\mu$ m-pore polyester membrane inserts (Corning, 3450), placed in 6-well plates and kept in 1 ml of NK differentiation medium as previously reported<sup>47</sup>. The medium was entirely refreshed every 2–3 days for 14 days.

At step III, on day 28, every four organoids were incubated with 1 ml of digestion buffer (1 mg ml<sup>-1</sup> collagenase type IV, 1 mg ml<sup>-1</sup> dispase and 50 UDNase I) for 15 min at 37 °C. Subsequently, the enzyme-treated organoids were carefully pipetted and filtered through a 70- $\mu$ m filter (Corning, 352350). After centrifugation, the cells were collected and cultured in a 1 l cell culture bag at 1 million cells per ml. Fresh medium was added to maintain the cell density at  $1 \times 10^6$ – $1.5 \times 10^6$  cells per ml. On day 35, cells in the cell culture bag were collected and transferred to new cell culture bags ( $1 \times 10^8$  cells per bag). Cells from a culture bag collected from day 35 were generally divided into 7–12 cell culture bags (100 million per bag) for the second round of bag-based NK proliferation. On day 42, mature iNK cells and CD19 CAR-iNK cells were collected for follow-up experiments or cryopreserved for future use.

For cryopreservation of iNK cells and CD19 CAR-iNK cells, cells were collected and cryopreserved with CryoStor CS10 cell-freezing medium (STEMCELL Technologies, 100-1061). Through controlled-rate freezing, iNK cells and CD19 CAR-iNK cells were eventually transferred to liquid nitrogen for long-term cryopreservation. For animal experiments, the cryopreserved cells were thawed, washed and immediately used for in vivo tumour suppression, aiming to recapitulate the clinical applications of off-the-shelf NK and CAR-NK cell products. Absolute CAR-NK cell counts were calculated by multiplying the total viable NK cells by their CAR ratios. For in vitro evaluation, cryopreserved cells were thawed, washed and cultured for 24, 48 and 72 h to dynamically evaluate their viability, cell number and specific cytotoxicity.

### Isolation and expansion of UCB-NK cells

CD3<sup>+</sup> umbilical cord blood mononuclear cells, purified using CD3 biotin (Biolegend, clone HIT3a), and the Anti-biotin MicroBeads UltraPure kit (Miltenyi Biotec, 130-090-485) were stimulated on day 0 with K562-mbIL-21 cells (Hangzhou Zhongying Biomedical, ZY-NKZ-0104) and rhIL-2 in KBM581 serum-free medium. On days 12–14, activated UCB-NK cells were cryopreserved or directly used for subsequent experiments.

### CD19 CAR<sup>+</sup> HSPC enrichment

CD19 CAR-HSPCs, comprising CD34<sup>+</sup> HSPCs infected with CD19 CAR retroviral vectors (MOI = 10) and expanded until day 7, were purified using CD19 CAR biotin (BioSwan, clone M19H) and the Anti-biotin MicroBeads UltraPure kit. Subsequently, the purified CD19 CAR<sup>+</sup> HSPCs underwent another 7-day HSPC expansion process.

### Antibodies and flow cytometry

Cells were initially treated with Human TruStain FcXTM to block Fc receptors and subsequently labelled with specific antibodies. The antibodies used for staining included CD3, CD7, CD16, CD19, CD34, CD45, CD56, CD319, NKp30, NKp44, NKG2D, CD69, CD94, NKG2A,



CD96, TRAIL, FasL, CD107a, TNF, IFN $\gamma$ , Perforin, GZMB, 2B4, DNAM-1, NKp46, anti-FMC63 scFv, CD161, CD328, PD-1, Tim-3, TIGIT, CD158a (KIR2DL1), CD158e1 (KIR3DL1, NKBI), CD158b/j (KIR2DL2/L3/S2) and KIR2DS4 (CD158i). Following staining, cells were resuspended in DAPI solution and analysed using the BD LSRFortessa X-20 cytometer (BD Biosciences). Flow cytometry data were acquired and analysed using FlowJo software (Tree Star). Detailed information on these antibodies is given in Supplementary Table 2.

### Vector copy number analysis

The genomic DNAs of iNK cells, CD19 CAR-iNK cells and CD19 CAR-UCB-NK cells were extracted using the TIAnamp Genomic DNA kit (TIANGEN, DP304). The CD19 CAR transgene was analysed as previously described<sup>62</sup>. Primers were designed to amplify a 148-bp fragment spanning part of the CD8 hinge region and part of the CD8 transmembrane region (Forward primer: 5'-ACCACTACTCCCGCTCCAAGGC-3', Reverse primer: 5'-GATCACGAGTGAAAGCAGCAGGACC-3', Probe: 5'-FAM- ACCATCGCCTCTCAGCCGCTTCCC-TAMRA-3'). SFG-CD19 CAR vectors ( $1 \times 10^9$  copies per  $\mu$ l) were used as the standard sample. A seven-point standard curve that consisted of  $5 \times 10^1$ – $5 \times 10^7$  copies per  $\mu$ l of SFG-CD19 CAR vectors was prepared. Quantitative real-time PCR was performed with 40 ng of genomic DNA in each reaction using Hieff Unicon qPCR TaqMan Probe Master Mix (YEASEN, 11205ES08), in a real-time PCR system (BIO-RAD, CFX Opus 96). VCN was calculated as previously reported<sup>63</sup>.

### RNA-seq and data analysis

Activated UCB-NK cells (day 14), iNK cells (day 42) and CD19 CAR-iNK cells (day 42) were subjected to single-cell RNA sequencing (10x Genomics), with 50,000 CD45<sup>+</sup>CD3<sup>+</sup>CD56<sup>+</sup> cells sorted per sample. Droplet-based scRNA-seq datasets were generated using a Chromium system (10x Genomics, PN120263) according to manufacturer instructions. Raw sequencing data from UCB-NK cells, iNK cells and CD19 CAR-iNK cells (HRA007978), as well as iPSC-iNK and ESC-iNK cells (HRA001609)<sup>17</sup>, were aligned and quantified using Cell Ranger (v.6.0.0), followed by analysis with Seurat (v.3.2.3). To pass quality control, cells had to detect at least 500 genes but <8,000 genes, and <10% of aligned reads were assigned to mitochondrial genes. A total of 5,368, 7,196, 9,033, 10,650 and 8,506 cells from UCB-NK cells, ESC-iNK cells, iPSC-iNK cells, iNK cells and CD19 CAR-iNK cells, respectively, were merged and used for downstream analysis.

Differential expression analysis to compare iNK cells with each of the UCB-NK cells, ESC-iNK cells, iPSC-iNK cells and CD19 CAR-iNK cells was performed using the 'MAST' test with the parameter 'min.pct = 0.25, logfc.threshold = 0.5'. GO enrichment analysis for differential gene expression was performed using the clusterProfiler package (v.4.2.2) with a BH-adjusted cut-off value of 0.05. Violin plots of the normalized expression of genes were plotted using the Seurat (v.3.2.3) and ggplot2 R packages.

Functions in Seurat (v.3.2.3) were used to integrate datasets. The 'SCTransform' function was applied for normalization. The 'SelectIntegrationFeatures' function was used to select 2,000 features for integration. Then, the 'FindIntegrationAnchors' function was utilized to find a set of anchors among the three scRNA-seq datasets using the selected features, with the parameter 'k.filter=100'. Finally, the 'IntegrateData' function was used to align the datasets, and the standard workflow for clustering and UMAP analysis was implemented using the first 20 principal components (PCs). Similarly, the datasets for UCB-NK cells, ESC-iNK cells, iPSC-iNK cells and iNK cells were integrated using the 'FindIntegrationAnchors' and 'IntegrateData' functions with the first 30 PCs to implement UMAP analysis.

### Perforin, GZMB, IFN $\gamma$ and TNF analysis

iNK cells and same-cord-blood expanded UCB-NK cells (effectors) were thawed at 4–6 days before the assays. PMA/ionomycin

(MULTISCIENCES, CS1001) and K562 cells were applied to analyse these proteins. For PMA/ionomycin, the effectors were stimulated with or without PMA/ionomycin for 2 h, followed by the addition of BFA/monensin (MULTISCIENCES, CS1002) for an additional 2-h incubation to analyse the expression levels of IFN $\gamma$  and TNF. NK cells for Perforin and GZMB analysis were directly used for staining without stimulation. The effectors were stimulated with K562 cells for 4 h, followed by the addition of BFA/monensin (MULTISCIENCES, CS1002) for an additional 4-h incubation to analyse the expression levels of Perforin, GZMB, IFN $\gamma$  and TNF by flow cytometry. Effectors were stimulated with K562 cells for 8 h to collect suspensions for ELISA analysis. ELISA kits used are QuantiCyto Human IFN $\gamma$  ELISA kit (NEOBIO SCIENCE, EHC102g.96), QuantiCyto Human TNF ELISA kit (NEOBIO SCIENCE, EHC103a.96), QuantiCyto Human Perforin ELISA kit (NEOBIO SCIENCE, EHC154.96) and QuantiCyto Human Granzyme B ELISA kit (NEOBIO SCIENCE, EHC117.96). The effectors were analysed using the BD LSRFortessa X-20 cytometer (BD Biosciences). Flow cytometry data were acquired and analysed using FlowJo software.

### Cytotoxicity and serial killing assays

iNK cells and same-cord blood expanded UCB-NK cells were thawed at 4–6 days before the cytotoxicity and serial killing assays. Effector cells (UCB-NK cells, iNK cells, CD19 CAR-UCB-NK cells and CD19 CAR-iNK cells) were incubated with eBioscience Cell Proliferation Dye eFluor 670 (eFluor 670; Invitrogen, 65-0840-85) labelled target cells (T) (K562, HL-60, NALM6, A1847, MOLM-13 or THP-1) in U-bottom 96-well plates at respective E:T ratios. In the serial target killing assay, effector cells were co-cultured with eFluor 670-labelled target cells (K562 or NALM6) at a ratio of 1:1 for three rounds (12 h per round). At the end of each round, effector cells (CD56<sup>+</sup>) were sorted for the next round of killing assay. We used the BD LSRFortessa flow cytometer or BD FACS Aria Fusion flow cytometer (BD Biosciences), determining the percentage of DAPI within the APC-positive population. Data were calculated using the formula: (percentage of tumour cell death – percentage of tumour cell spontaneous death) / (1 – percentage of tumour cell spontaneous death)  $\times$  100.

### Isolation of primary patient-derived B-cell lymphoma cells and patient-derived B-cell leukaemia cells

To isolate B lymphoma cells, tumour tissues isolated from patients were mechanically separated into 1 mm  $\times$  1 mm fragments after washing with PBS. The fragments were then subjected to enzyme digestion using digestion buffer (1 mg ml<sup>-1</sup> collagenase type IV, 1 mg ml<sup>-1</sup> dispase and 50 U DNase I) at 37 °C for 30 min. The resulting cell suspension was then centrifuged and filtered to obtain a single-cell suspension of the desired cells. Mononuclear cells were isolated using Ficoll-Hypaque density gradient centrifugation to isolate B-cell leukaemia cells from patient samples.

### Construction of ovarian cancer xenograft models and treatment with iNK cells

NCG mice were injected intraperitoneally with A1847-luci<sup>+</sup> cells ( $2 \times 10^5$  cells per mouse) on day -1 to establish models of ovarian cancer xenografts. BLI imaging (IVIS Spectrum, PerkinElmer) was performed to quantify the tumour burden, and models with similar total flux (p s<sup>-1</sup>) were randomly divided into three groups (tumour-only, tumour + UCB-NK and tumour + iNK) on day 0. These models were first irradiated (2.25 Gy, Rad Source RS2000). The irradiated mice were intraperitoneally injected with iNK cells or UCB-NK cells ( $1.5 \times 10^7$  cells per mouse) on days 0 and 7. BLI was performed to track the tumour cells every week. Mice suffering from heavy tumour burdens were killed for ethical considerations.

### Construction of B-ALL xenograft models and CD19 CAR-iNK cell treatment

B-NDG hL15 mice were established as ALL xenograft models by intravenously injecting NALM6-luci<sup>+</sup> cells ( $1 \times 10^5$  cells per mouse) on day

–1. On day 0, tumour burdens were quantified using bioluminescence imaging (IVIS Spectrum, PerkinElmer). Mice were irradiated (1.5 Gy, Rad Source RS2000), intravenously injected with PBS, iNK cells, CD19 CAR-UCB-NK cells or CD19 CAR-iNK cells ( $\sim 1 \times 10^7$  CD19 CAR<sup>+</sup> cells per mouse), and then given a second injection on day 3. rhIL-2 (10,000 IU per mouse, Miltenyi Biotec) was administered every 2 days until day 14 post NK cell injection. Weekly BLI assessments were conducted to monitor tumour progression. Mice with heavy tumour burdens were killed according to ethical guidelines.

### Construction of patient-derived B-ALL xenograft models and CD19 CAR-iNK cell treatment

Patient-derived primary B-ALL (FLT3-TKD, MLL-ENL) cells (5 million per mouse) were intravenously injected into B-NDG mice to obtain enough fresh proliferating cells for in vitro and in vivo assays. At 6 weeks post injection, the spleens of these mice were ground to collect single cells. The patient-derived B-ALL primary cells were immediately infected with Luciferase-tdTomato lentivirus particles (MOI = 10) using Vectofusin-1 (Miltenyi, 130-111-163). At 72 h post infection (day –1), luciferase-expressing (CD19<sup>+</sup>tdTomato<sup>+</sup>) patient-derived B-ALL cells (B-ALL luci<sup>+</sup>) were sorted and intravenously injected ( $2 \times 10^6$  cells per mouse) into B-NDG hIL15 mice to construct PDX models. Mice were intravenously injected with iNK cells, CD19 CAR-UCB-NK cells or CD19 CAR-iNK cells ( $\sim 1 \times 10^7$  CD19 CAR<sup>+</sup> cells per mouse), and then a second injection was performed on day 3. Mice with heavy tumour burdens (CD19<sup>+</sup> cells in PB >50%) were killed to alleviate suffering due to splenomegaly.

### Statistics

All quantitative analyses were performed with SPSS (v.23). Data are depicted as mean  $\pm$  s.d., and statistical tests used are described in detail in the figure legends.

### Reporting summary

Further information on research design is available in the Nature Portfolio Reporting Summary linked to this article.

### Data availability

Single-cell RNA sequencing data (UCB-NK, iNK and CD19 CAR-iNK) (fastq files) have been uploaded to the Genome Sequence Archive (HRA007978) (<https://ngdc.cncb.ac.cn/gsa-human/browse/HRA007978>)<sup>64</sup>. Single-cell RNA sequencing data (iPSC-iNK, ESC-iNK)<sup>17</sup> were downloaded from the Genome Sequence Archive (HRA001609) (<https://ngdc.cncb.ac.cn/gsa-human/browse/HRA001609>). The main data supporting the results in this study are available within the paper and its Supplementary Information. The corresponding author (J.W.) will make raw data and step-by-step protocols available upon request. Source data for the figures are provided with this paper.

### Code availability

R scripts with .R files used to analyse scRNA-seq data have been deposited on Zenodo at <https://doi.org/10.5281/zenodo.15787629> (ref 65).

### References

- Larson, R. C. & Maus, M. V. Recent advances and discoveries in the mechanisms and functions of CAR T cells. *Nat. Rev. Cancer* **21**, 145–161 (2021).
- Laskowski, T. J., Biederstadt, A. & Rezvani, K. Natural killer cells in antitumour adoptive cell immunotherapy. *Nat. Rev. Cancer* **22**, 557–575 (2022).
- Vivier, E. et al. Natural killer cell therapies. *Nature* **626**, 727–736 (2024).
- Cichocki, F. & Miller, J. S. In vitro development of human killer-immunoglobulin receptor-positive NK cells. *Methods Mol. Biol.* **612**, 15–26 (2010).
- Gong, Y., Klein Wolterink, R. G. J., Wang, J., Bos, G. M. J. & Germeraad, W. T. V. Chimeric antigen receptor natural killer (CAR-NK) cell design and engineering for cancer therapy. *J. Hematol. Oncol.* **14**, 73 (2021).
- Zhang, Y. et al. In vivo kinetics of human natural killer cells: the effects of ageing and acute and chronic viral infection. *Immunology* **121**, 258–265 (2007).
- Page, A., Chuvin, N., Valladeau-Guilemond, J. & Depil, S. Development of NK cell-based cancer immunotherapies through receptor engineering. *Cell. Mol. Immunol.* **21**, 315–331 (2024).
- Liu, E. et al. Use of CAR-transduced natural killer cells in CD19-positive lymphoid tumors. *N. Engl. J. Med.* **382**, 545–553 (2020).
- Marin, D. et al. Safety, efficacy and determinants of response of allogeneic CD19-specific CAR-NK cells in CD19<sup>+</sup> B cell tumors: a phase 1/2 trial. *Nat. Med.* **30**, 772–784 (2024).
- de Jonge, P. et al. Good manufacturing practice production of CD34<sup>+</sup> progenitor-derived NK cells for adoptive immunotherapy in acute myeloid leukemia. *Cancer Immunol. Immunother.* **72**, 3323–3335 (2023).
- Myers, J. A. & Miller, J. S. Exploring the NK cell platform for cancer immunotherapy. *Nat. Rev. Clin. Oncol.* **18**, 85–100 (2021).
- De Oliveira, S. N. et al. Modification of hematopoietic stem/progenitor cells with CD19-specific chimeric antigen receptors as a novel approach for cancer immunotherapy. *Hum. Gene Ther.* **24**, 824–839 (2013).
- Albert, S. et al. Tonic signaling and its effects on lymphopoiesis of CAR-armed hematopoietic stem and progenitor cells. *J. Immunol.* **202**, 1735–1746 (2019).
- Moore, K. A., Ema, H. & Lemischka, I. R. In vitro maintenance of highly purified, transplantable hematopoietic stem cells. *Blood* **89**, 4337–4347 (1997).
- Fares, I. et al. Cord blood expansion. Pyrimidoindole derivatives are agonists of human hematopoietic stem cell self-renewal. *Science* **345**, 1509–1512 (2014).
- Montel-Hagen, A. et al. Organoid-induced differentiation of conventional T cells from human pluripotent stem cells. *Cell Stem Cell* **24**, 376–389.e8 (2019).
- Huang, D. et al. Lateral plate mesoderm cell-based organoid system for NK cell regeneration from human pluripotent stem cells. *Cell Discov.* **8**, 121 (2022).
- Riviere, I., Brose, K. & Mulligan, R. C. Effects of retroviral vector design on expression of human adenosine deaminase in murine bone marrow transplant recipients engrafted with genetically modified cells. *Proc. Natl. Acad. Sci. USA* **92**, 6733–6737 (1995).
- Bueler, H. & Mulligan, R. C. Induction of antigen-specific tumor immunity by genetic and cellular vaccines against MAGE: enhanced tumor protection by coexpression of granulocyte-macrophage colony-stimulating factor and B7-1. *Mol. Med.* **2**, 545–555 (1996).
- Thiemann, F. T., Moore, K. A., Smogorzewska, E. M., Lemischka, I. R. & Crooks, G. M. The murine stromal cell line AFT024 acts specifically on human CD34<sup>+</sup>CD38<sup>–</sup> progenitors to maintain primitive function and immunophenotype in vitro. *Exp. Hematol.* **26**, 612–619 (1998).
- Punzel, M., Gupta, P., Roodell, M., Mortari, F. & Verfaillie, C. M. Factor(s) secreted by AFT024 fetal liver cells following stimulation with human cytokines are important for human LTC-IC growth. *Leukemia* **13**, 1079–1084 (1999).
- Nolta, J. A. et al. The AFT024 stromal cell line supports long-term ex vivo maintenance of engrafting multipotent human hematopoietic progenitors. *Leukemia* **16**, 352–361 (2002).
- Chen, Y. et al. ADGRG1 enriches for functional human hematopoietic stem cells following ex vivo expansion-induced mitochondrial oxidative stress. *J. Clin. Invest.* **131**, e148329 (2021).

24. Chen, J. et al. Tuning charge density of chimeric antigen receptor optimizes tonic signaling and CAR-T cell fitness. *Cell Res.* **33**, 341–354 (2023).
25. Beziat, V. et al. Tracing dynamic expansion of human NK-cell subsets by high-resolution analysis of KIR repertoires and cellular differentiation. *Eur. J. Immunol.* **44**, 2192–2196 (2014).
26. Hsu, K. C. et al. Improved outcome in HLA-identical sibling hematopoietic stem-cell transplantation for acute myelogenous leukemia predicted by KIR and HLA genotypes. *Blood* **105**, 4878–4884 (2005).
27. Wang, Y. et al. Comparison of seven CD19 CAR designs in engineering NK cells for enhancing anti-tumour activity. *Cell Prolif.* **57**, e13683 (2024).
28. Bryceson, Y. T., March, M. E., Ljunggren, H. G. & Long, E. O. Activation, coactivation, and costimulation of resting human natural killer cells. *Immunol. Rev.* **214**, 73–91 (2006).
29. Quatrini, L. et al. Human NK cells, their receptors and function. *Eur. J. Immunol.* **51**, 1566–1579 (2021).
30. Prager, I. & Watzl, C. Mechanisms of natural killer cell-mediated cellular cytotoxicity. *J. Leukoc. Biol.* **105**, 1319–1329 (2019).
31. Alter, G., Malenfant, J. M. & Altfeld, M. CD107a as a functional marker for the identification of natural killer cell activity. *J. Immunol. Methods* **294**, 15–22 (2004).
32. Di Santo, J. P. Functionally distinct NK-cell subsets: developmental origins and biological implications. *Eur. J. Immunol.* **38**, 2948–2951 (2008).
33. Voskoboinik, I., Whisstock, J. C. & Trapani, J. A. Perforin and granzymes: function, dysfunction and human pathology. *Nat. Rev. Immunol.* **15**, 388–400 (2015).
34. Franks, S. E., Wolfson, B. & Hodge, J. W. Natural born killers: NK cells in cancer therapy. *Cancers* **12**, 2131 (2020).
35. Woan, K. V. et al. Harnessing features of adaptive NK cells to generate iPSC-derived NK cells for enhanced immunotherapy. *Cell Stem Cell* **28**, 2062–2075.e5 (2021).
36. Vankayalapati, R. et al. Role of NK cell-activating receptors and their ligands in the lysis of mononuclear phagocytes infected with an intracellular bacterium. *J. Immunol.* **175**, 4611–4617 (2005).
37. Sivori, S. et al. Inhibitory receptors and checkpoints in human NK cells, implications for the immunotherapy of cancer. *Front. Immunol.* **11**, 2156 (2020).
38. Zhang, Q. et al. Blockade of the checkpoint receptor TIGIT prevents NK cell exhaustion and elicits potent anti-tumor immunity. *Nat. Immunol.* **19**, 723–732 (2018).
39. Li, Y., Mateu, E. & Diaz, I. Impact of cryopreservation on viability, phenotype, and functionality of porcine PBMC. *Front. Immunol.* **12**, 765667 (2021).
40. Baumeister, S. H. et al. Phase I trial of autologous CAR T cells targeting NKG2D ligands in patients with AML/MDS and multiple myeloma. *Cancer Immunol. Res.* **7**, 100–112 (2019).
41. Derigs, P. et al. Third-generation anti-CD19 CAR T cells for relapsed/refractory chronic lymphocytic leukemia: a phase 1/2 study. *Leukemia* **38**, 2419–2428 (2024).
42. Liu, E. et al. Cord blood NK cells engineered to express IL-15 and a CD19-targeted CAR show long-term persistence and potent antitumor activity. *Leukemia* **32**, 520–531 (2018).
43. Levine, B. L. et al. Unanswered questions following reports of secondary malignancies after CAR-T cell therapy. *Nat. Med.* **30**, 338–341 (2024).
44. Wineman, J., Moore, K., Lemischka, I. & Muller-Sieburg, C. Functional heterogeneity of the hematopoietic microenvironment: rare stromal elements maintain long-term repopulating stem cells. *Blood* **87**, 4082–4090 (1996).
45. Yoshida, H. et al. The murine mutation osteopetrosis is in the coding region of the macrophage colony stimulating factor gene. *Nature* **345**, 442–444 (1990).
46. Kodama, H., Nose, M., Niida, S., Nishikawa, S. & Nishikawa, S. Involvement of the c-kit receptor in the adhesion of hematopoietic stem cells to stromal cells. *Exp. Hematol.* **22**, 979–984 (1994).
47. Nakano, T., Kodama, H. & Honjo, T. Generation of lymphohematopoietic cells from embryonic stem cells in culture. *Science* **265**, 1098–1101 (1994).
48. Nakano, T. Lymphohematopoietic development from embryonic stem cells in vitro. *Semin. Immunol.* **7**, 197–203 (1995).
49. Moore, K. A., Pytowski, B., Witte, L., Hicklin, D. & Lemischka, I. R. Hematopoietic activity of a stromal cell transmembrane protein containing epidermal growth factor-like repeat motifs. *Proc. Natl. Acad. Sci. USA* **94**, 4011–4016 (1997).
50. Zanetti, C. & Krause, D. S. ‘Caught in the net’: the extracellular matrix of the bone marrow in normal hematopoiesis and leukemia. *Exp. Hematol.* **89**, 13–25 (2020).
51. Takakura, N., Kodama, H., Nishikawa, S. & Nishikawa, S. Preferential proliferation of murine colony-forming units in culture in a chemically defined condition with a macrophage colony-stimulating factor-negative stromal cell clone. *J. Exp. Med.* **184**, 2301–2309 (1996).
52. Figueiredo, L. M., Costa, E. B., Orellana, M. D., Picanco-Castro, V. & Covas, D. T. OP9 stromal cells proteins involved in hematoendothelial differentiation from human embryonic stem cells. *Cell. Reprogram.* **17**, 338–346 (2015).
53. Donnelly, H. et al. Bioengineered niches that recreate physiological extracellular matrix organisation to support long-term haematopoietic stem cells. *Nat. Commun.* **15**, 5791 (2024).
54. Wu, Q. et al. Signal via lymphotoxin-beta R on bone marrow stromal cells is required for an early checkpoint of NK cell development. *J. Immunol.* **166**, 1684–1689 (2001).
55. Roth, C., Rothlin, C., Riou, S., Raulet, D. H. & Lemke, G. Stromal-cell regulation of natural killer cell differentiation. *J. Mol. Med.* **85**, 1047–1056 (2007).
56. Brewin, J. et al. Generation of EBV-specific cytotoxic T cells that are resistant to calcineurin inhibitors for the treatment of posttransplantation lymphoproliferative disease. *Blood* **114**, 4792–4803 (2009).
57. Cosset, F. L., Takeuchi, Y., Battini, J. L., Weiss, R. A. & Collins, M. K. High-titer packaging cells producing recombinant retroviruses resistant to human serum. *J. Virol.* **69**, 7430–7436 (1995).
58. Wang, Y. et al. Identification of stem cells after transplantation. *Methods Mol. Biol.* **1036**, 89–94 (2013).
59. Ngom, M. et al. UM171 enhances lentiviral gene transfer and recovery of primitive human hematopoietic cells. *Mol. Ther. Methods Clin. Dev.* **10**, 156–164 (2018).
60. Kelly, P. F., Vandergriff, J., Nathwani, A., Nienhuis, A. W. & Vanin, E. F. Highly efficient gene transfer into cord blood nonobese diabetic/severe combined immunodeficiency repopulating cells by oncoretroviral vector particles pseudotyped with the feline endogenous retrovirus (RD114) envelope protein. *Blood* **96**, 1206–1214 (2000).
61. Majdoul, S. et al. Molecular determinants of vectofusin-1 and its derivatives for the enhancement of lentivirally mediated gene transfer into hematopoietic stem/progenitor cells. *J. Biol. Chem.* **291**, 2161–2169 (2016).
62. Till, B. G. et al. CD20-specific adoptive immunotherapy for lymphoma using a chimeric antigen receptor with both CD28 and 4-1BB domains: pilot clinical trial results. *Blood* **119**, 3940–3950 (2012).



63. Haderbach, R. et al. Droplet digital PCR allows vector copy number assessment and monitoring of experimental CAR T cells in murine xenograft models or approved CD19 CAR T cell-treated patients. *J. Transl. Med.* **19**, 265 (2021).
64. Hu, F. et al. hspc\_iNK. Dataset. *Genome Sequence Archive* <https://ngdc.cncb.ac.cn/gsa-human/browse/HRA007978> (2025).
65. Hu, F. et al. scRNAseq\_UCB\_HSPC\_iNK. Source code. *Zenodo* <https://doi.org/10.5281/zenodo.15787629> (2025).

## Acknowledgements

We thank J. Zhang (SPF-grade animal facilities at the Guangzhou Institutes of Biomedicine and Health, Chinese Academy of Sciences) for cell injection and bioluminescence imaging assays. This work was supported by grants from the National Key R&D Program of China (2024YFA1108302 to J.W. and 2020YFA0112404 to J.W.), the National Natural Science Foundation of China (82450001 to J.W., 81925002 to J.W., 82300132 to D.H.), and the Noncommunicable Chronic Diseases-National Science and Technology Major Project (No. 2023ZD0501200 to J.W.).

## Author contributions

J.W. and F.H. designed the project. F.H., J.L., Y.W., Y.L. and J.Z. contributed equally. F.H. designed the experiments. F.H., J.L. and Y.W. performed all experiments. J.Z. provided the B-ALL patient-derived primary cells and participated in the PDX experiments. J.W., F.H., J.L. and M.Z. wrote the paper. Y.L. and Q.W. analysed the RNA-seq data. J.X., Y.L., X. Zheng, X.L., Y.G., H.W., L.L., H.P., B.W., D.H., C.X. and T.W. participated in multiple experiments. X.D., H.Z., F.D., Y.Z., X. Zhu and M.Z. discussed the data and paper. J.W. provided the final approval of the paper.

## Competing interests

The authors declare no competing interests.

## Additional information

**Extended data** is available for this paper at <https://doi.org/10.1038/s41551-025-01522-5>.

**Supplementary information** The online version contains supplementary material available at <https://doi.org/10.1038/s41551-025-01522-5>.

**Correspondence and requests for materials** should be addressed to Xiaofan Zhu, Mengyun Zhang or Jinyong Wang.

**Peer review information** *Nature Biomedical Engineering* thanks Katy Rezvani and the other, anonymous, reviewer(s) for their contribution to the peer review of this work.

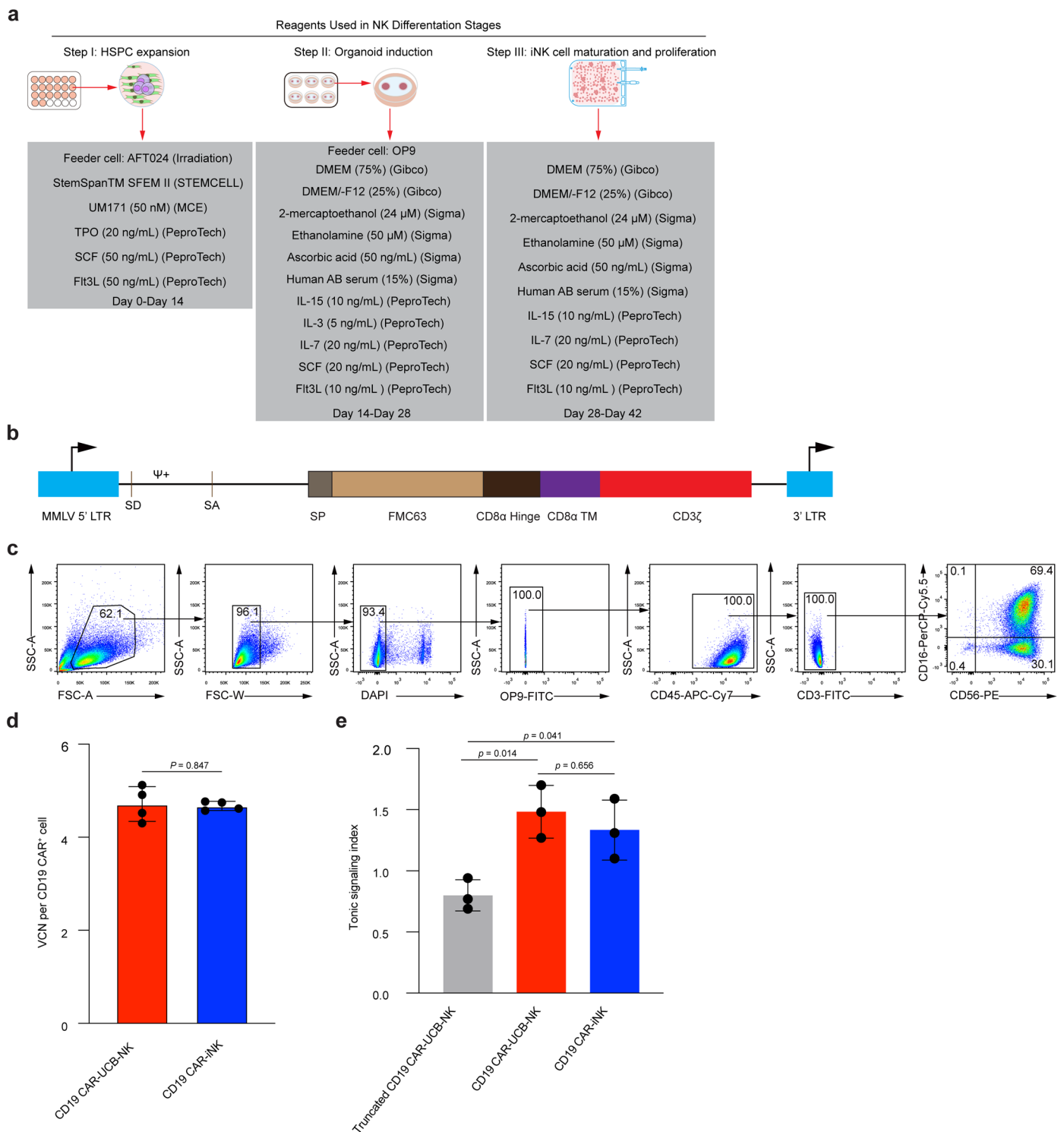
**Reprints and permissions information** is available at [www.nature.com/reprints](http://www.nature.com/reprints).

**Publisher's note** Springer Nature remains neutral with regard to jurisdictional claims in published maps and institutional affiliations.

Springer Nature or its licensor (e.g. a society or other partner) holds exclusive rights to this article under a publishing agreement with the author(s) or other rightsholder(s); author self-archiving of the accepted manuscript version of this article is solely governed by the terms of such publishing agreement and applicable law.

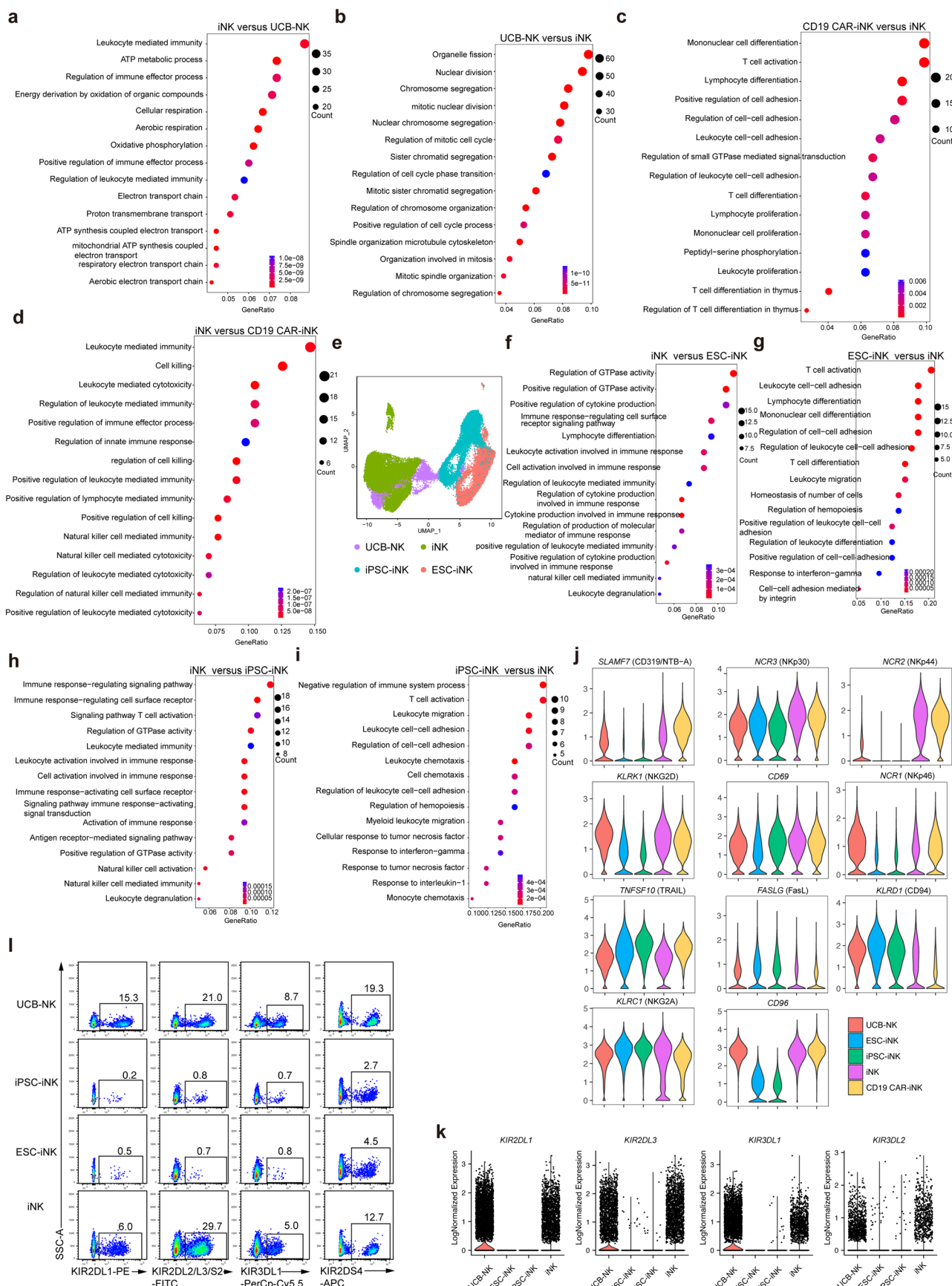
© The Author(s), under exclusive licence to Springer Nature Limited 2025

<sup>1</sup>State Key Laboratory of Organ Regeneration and Reconstruction, Institute of Zoology, Chinese Academy of Sciences, Beijing, China. <sup>2</sup>Beijing Institute for Stem Cell and Regenerative Medicine, Beijing, China. <sup>3</sup>Guangzhou Institutes of Biomedicine and Health, Chinese Academy of Sciences, Guangzhou, China. <sup>4</sup>University of Chinese Academy of Sciences, Beijing, China. <sup>5</sup>State Key Laboratory of Experimental Hematology, National Clinical Research Center for Blood Diseases, Haihe Laboratory of Cell Ecosystem, Institute of Hematology and Blood Diseases Hospital, Chinese Academy of Medical Sciences and Peking Union Medical College, Tianjin, China. <sup>6</sup>Guangdong Provincial People's Hospital, Guangzhou, China. <sup>7</sup>Department of Hematology, Guangdong Provincial People's Hospital (Guangdong Academy of Medical Sciences), Southern Medical University, Guangzhou, China. <sup>8</sup>These authors contributed equally: Fangxiao Hu, Jianhuan Li, Yao Wang, Yunqing Lin, Jingliao Zhang. ✉e-mail: [xfzhu@ihcams.ac.cn](mailto:xfzhu@ihcams.ac.cn); [zhangmengyun@ioz.ac.cn](mailto:zhangmengyun@ioz.ac.cn); [wangjinyong@ioz.ac.cn](mailto:wangjinyong@ioz.ac.cn)



**Extended Data Fig. 1 | Immune phenotypes and yields of iNK cells and CD19 CAR-iNK cells after 3-week bag-based culture. a**, The schematic diagram shows the reagents used in the NK induction protocol. **b**, Schematic of the genetic construct of SFG-CD19 CAR. Depicted are the 5' LTR promoter, packaging signal  $\Psi$ +, splice donor (SD), splice acceptor (SA), signal peptide (SP), anti-CD19 scFv (FMC63), CD8 $\alpha$  Hinge, CD8 $\alpha$  TM, and CD3 $\zeta$ . **c**, Example flow cytometry analysis of iNK cell populations induced from CD34<sup>+</sup> HSPCs. **d**, Statistical analysis of the CD19 CAR retroviral vector copy number in CD19 CAR-iNK cells and the same

donor-generated CD19 CAR-UCB-NK cells ( $n = 4$  in each group). **e**, Statistical analysis of the tonic signaling index of CD19 CAR-iNK cells, the same donor-generated CD19 CAR-UCB-NK cells, and the same donor-generated CD19 CAR-without-CD3 $\zeta$ -UCB-NK cells ( $n = 3$  in each group). Data were presented as mean  $\pm$  SD of four independent biological replicates (**d**) or three independent biological replicates (**e**).  $P$  values were calculated using unpaired two-sided  $t$ -test (**d**) or one-way ANOVA test with Tukey's multiple comparisons test (**e**). Exact  $P$  values are labelled.

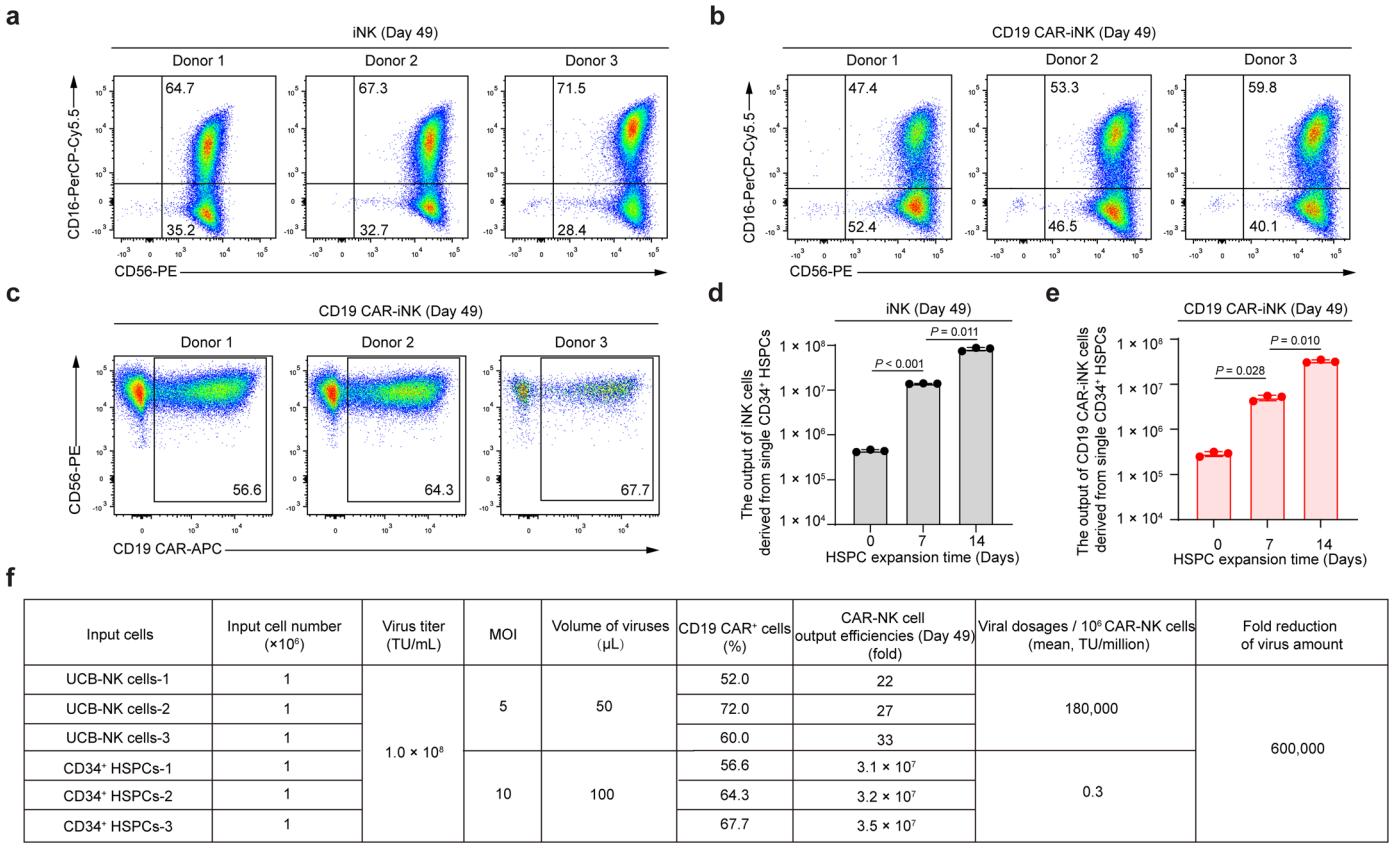


Extended Data Fig. 2 | See next page for caption.



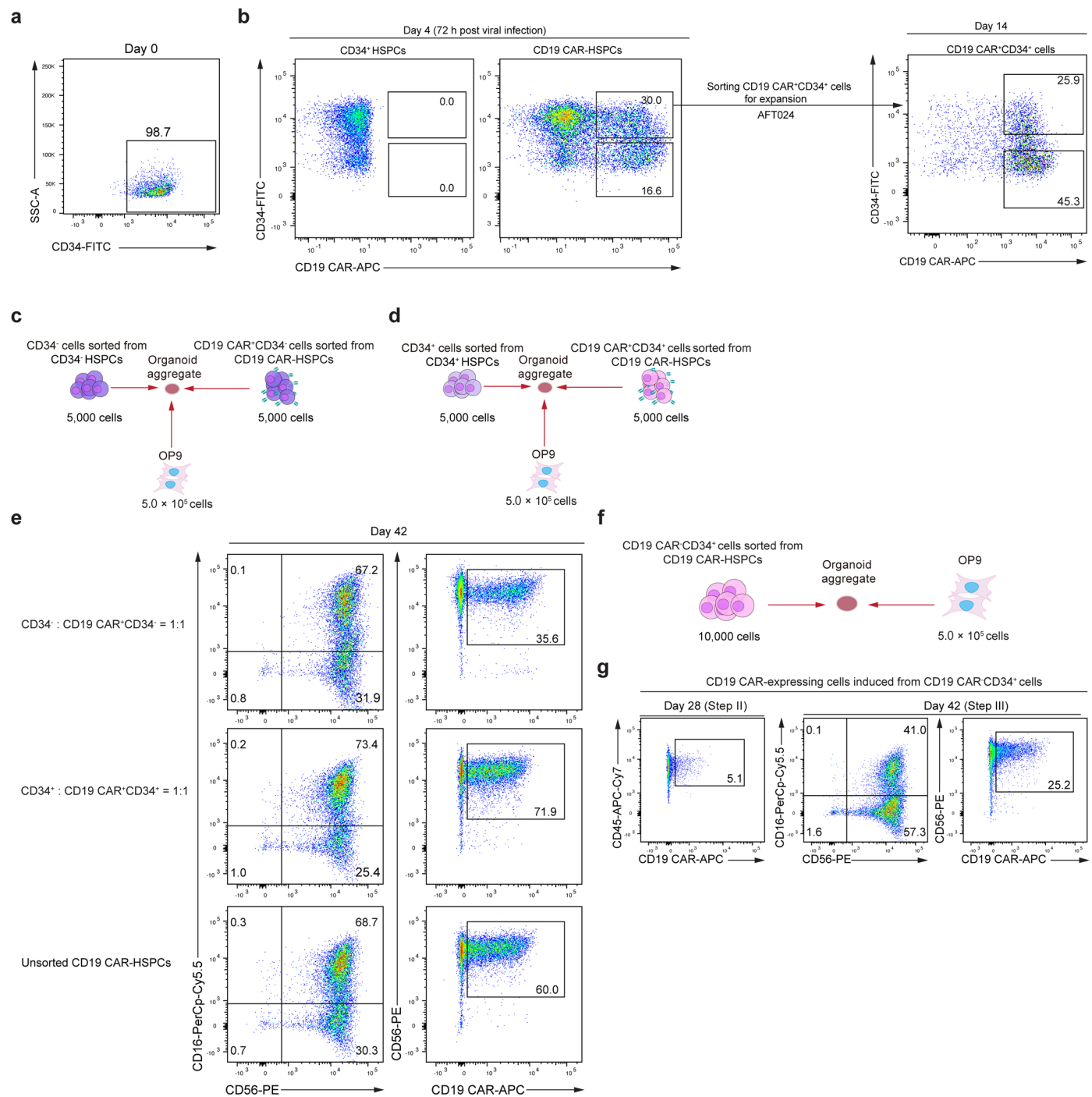
**Extended Data Fig. 2 | Characterization of the transcriptome features of CD19 CAR-iNK cells.** **a**, GO enrichment analysis of the upregulated genes in iNK cells compared with UCB-NK cells. **b**, GO enrichment analysis of the upregulated genes in UCB-NK cells compared with iNK cells. **c**, GO enrichment analysis of the upregulated genes in CD19 CAR-iNK cells compared with iNK cells. **d**, GO enrichment analysis of the upregulated genes in iNK cells compared with CD19 CAR-iNK cells. **e**, UMAP plots show the projections among UCB-NK, iNK, iPSC-iNK, and ESC-iNK cells. **f**, GO enrichment analysis of the upregulated genes in iNK cells compared with ESC-iNK cells. **g**, GO enrichment analysis of the

upregulated genes in ESC-iNK cells compared with iNK cells. **h**, GO enrichment analysis of the upregulated genes in iNK cells compared with iPSC-iNK cells. **i**, GO enrichment analysis of the upregulated genes in iPSC-iNK cells compared with iNK cells. **j**, Violin plots of the gene expression levels of *SLAMF7*, *NCR3*, *NCR2*, *KLRK1*, *CD69*, *KLRD1*, *KLRC1*, *CD96*, *NCRI*, *TNFSF10*, and *FASLG*. **k**, Violin plots of *KIR2DL1*, *KIR2DL3*, *KIR3DL1*, and *KIR3DL2* gene expression levels. **l**, Flow cytometric analysis of the KIR2DL1, KIR2DL2/L3/S2, KIR3DL1, and KIR2DS4 in UCB-NK cells, iPSC-iNK cells, ESC-iNK cells, and iNK cells.



**Extended Data Fig. 3 | Immune phenotypes and yields of iNK cells and CD19 CAR-iNK cells after 4-week bag-based culture.** **a,b**, Flow cytometric analysis of the immune phenotypes of iNK cells (**a**) and CD19 CAR-iNK cells (**b**) (CD56<sup>+</sup>CD16<sup>+</sup>). Data were collected from three donor umbilical cord blood units. **c**, Flow cytometric analysis of CD19 CAR expression (CD56<sup>+</sup>CD19 CAR<sup>+</sup>). **d,e**, Statistical analysis of the output efficiencies of iNK cells (CD45<sup>+</sup>CD3<sup>+</sup>CD56<sup>+</sup>CD16<sup>+</sup>) ( $n = 3$  in each group,  $n$  indicated three donor umbilical cord blood units) (**d**) or CD19 CAR-iNK cells (CD45<sup>+</sup>CD3<sup>+</sup>CD56<sup>+</sup>CD16<sup>+</sup>

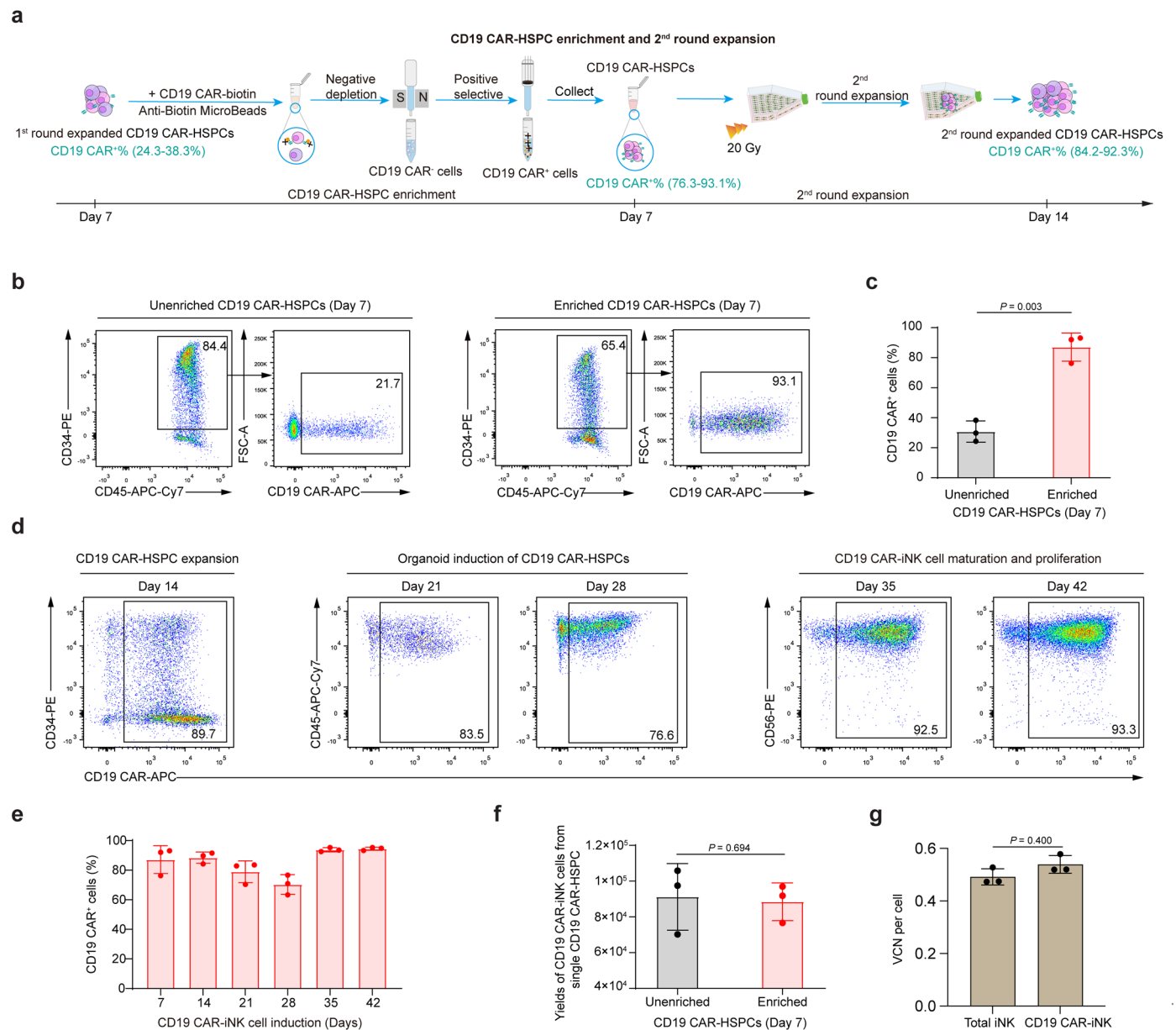
<sup>+</sup>CD19 CAR<sup>+</sup>) ( $n = 3$  in each group,  $n$  indicated three donor umbilical cord blood units) (**e**) derived from single CD34<sup>+</sup> HSPCs. Day 0, fresh CD34<sup>+</sup> HSPCs. Day 7, 7-day expanded CD34<sup>+</sup> HSPCs. Day 14, 14-day expanded CD34<sup>+</sup> HSPCs. Data were presented as mean  $\pm$  SD of independent biological replicates.  $P$  values were calculated using one-way ANOVA test with Tamhane T2's multiple comparisons test (**d** and **e**). Exact  $P$  values are labelled. **f**, Table showing the calculated quantities of CD19 CAR retroviruses (TU). The viral particles required to generate  $1.0 \times 10^6$  CD19 CAR-iNK cells and CD19 CAR-UCB-NK cells were compared.



**Extended Data Fig. 4 | CD19 CAR<sup>+</sup>CD34<sup>+</sup> cells were from CD19 CAR<sup>+</sup>CD34<sup>+</sup> HSPCs and retained the CAR-iNK cells' differentiation ability.** **a**, Flow cytometric analysis of the ratio of CD34<sup>+</sup> cells in CD34<sup>+</sup> HSPCs (CD34 MicroBead Kit enriched) on Day 0. **b**, Flow cytometric analysis of CD19 CAR-HSPCs on Day 4 and Day 14. HSPCs were transduced with CD19 CAR retroviral vectors after 72 h (Day 4). The sorted CD19 CAR<sup>+</sup>CD34<sup>+</sup> cells were expanded for 10 days using AFT024 cells (Day 14). **c**, Schematic diagram of the generation of organoid aggregate for iNK induction using sorted untransduced CD34<sup>+</sup> cells (5,000 cells/organoid)

(Day 14) and sorted CD19 CAR<sup>+</sup>CD34<sup>+</sup> cells (5,000 cells/organoid) (Day 14). **d**, Schematic diagram of the generation of organoid aggregate for iNK induction using sorted untransduced CD34<sup>+</sup> cells (5,000 cells/organoid) and sorted CD19 CAR<sup>+</sup>CD34<sup>+</sup> cells (5,000 cells/organoid) (Day 14). **e**, Flow cytometric analysis of CD19 CAR-iNK cells on Day 42. **f**, Schematic diagram of the generation of organoid aggregate for iNK induction using CD19 CAR<sup>+</sup>CD34<sup>+</sup> cells sorted from CD19 CAR-HSPCs on Day 14. **g**, Flow cytometric analysis of the expression of CD19 CAR in CD45<sup>+</sup> cells (Day 28) and CD56<sup>+</sup> cells (Day 42).

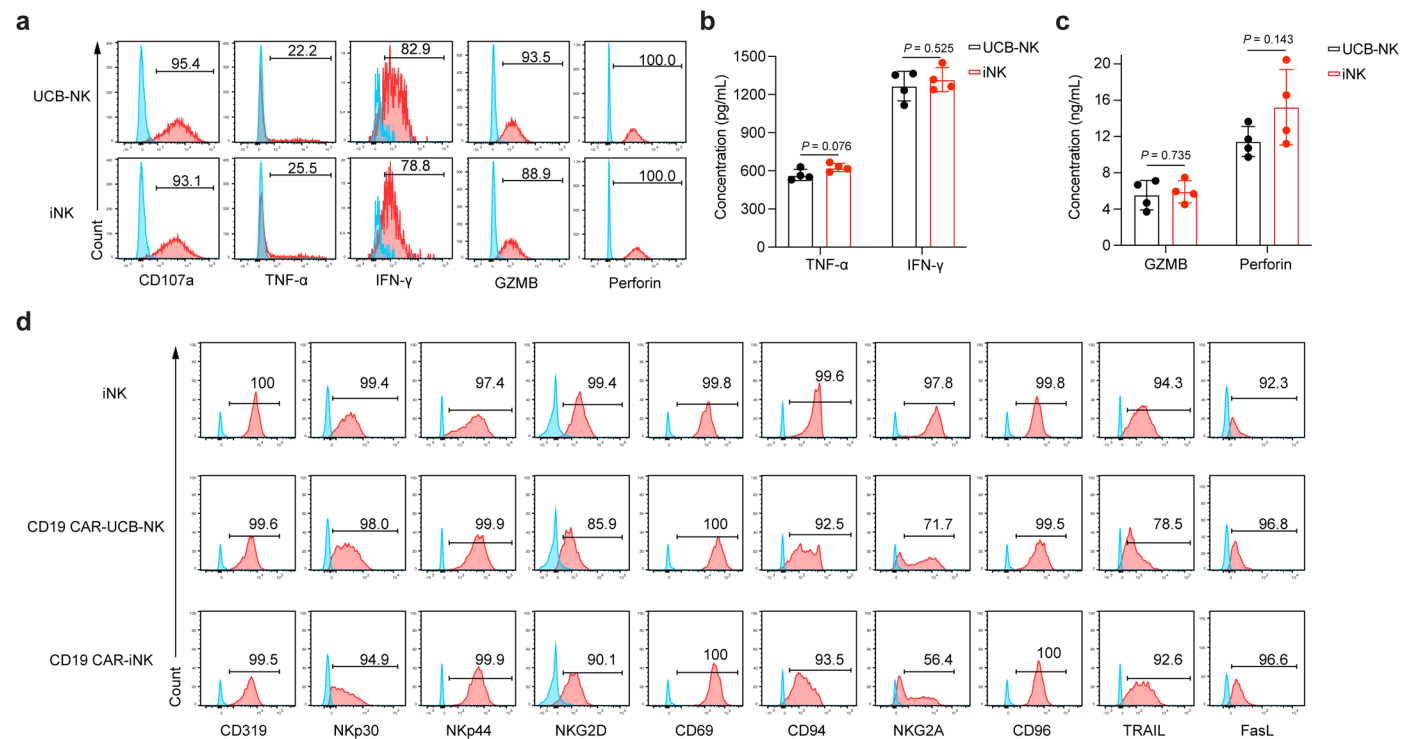




**Extended Data Fig. 5 | Enrichment of CD19 CAR<sup>+</sup> CD34<sup>+</sup> HSPCs on Day 7 further increased the positive CD19 CAR ratios of CD19 CAR-iNK cells on Day 42 by more than 90%.**

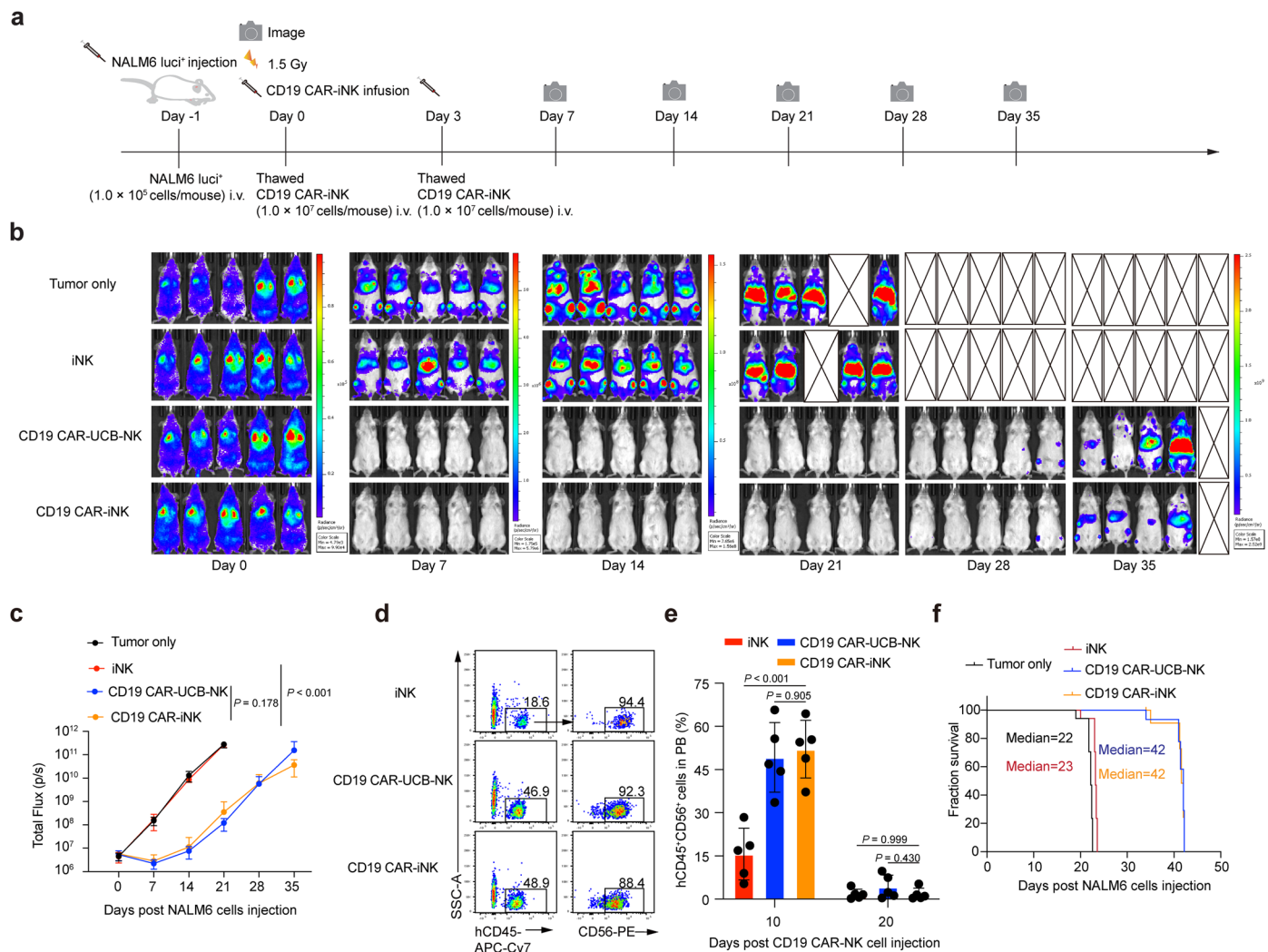
**a**, Schematic diagram of the generation of CD19 CAR<sup>+</sup> HSPCs from expanded 7-day CD19 CAR-HSPCs. **b**, Flow cytometric analysis of the CD19 CAR expression in CD34<sup>+</sup> HSPCs before and after enrichment using a CD19 CAR-based microbead enrichment process on Day 7. **c**, Statistical analysis of CD19 CAR expression levels in CD34<sup>+</sup> HSPCs before and after enrichment ( $n = 3$  in each group,  $n$  indicated three donor umbilical cord blood units). **d**, Representative FACS plots showing the expression of CD19 CAR in total cells at the indicated time points. **e**, Statistical analysis of the CD45<sup>+</sup> CD19 CAR<sup>+</sup> cell ratios at the

indicated time points. ( $n = 3$  in each group,  $n$  indicated three donor umbilical cord blood units). **f**, Statistical analysis of the yields of CD19 CAR-iNK cells from single 7-day expanded CD19 CAR-HSPCs ( $n = 3$  in each group,  $n$  indicated three donor umbilical cord blood units). **g**, CD19 CAR vector copy numbers in total iNK cells induced from enriched CD19 CAR-HSPCs or CD19 CAR-expressing iNK cells ( $n = 3$  in each group). Data were presented as mean  $\pm$  SD of three independent biological replicates (**e** and **f**) or three technical repeats from the same experimental unit (**g**), representative of two independent experiments.  $P$  values were calculated using paired two-sided  $t$ -test (**c** and **f**) or two-sided Mann-Whitney U test (**g**). Exact  $P$  values are labelled.



**Extended Data Fig. 6 | Evaluation of the secretome expressed in iNK cells and the phenotypes of CD19 CAR-iNK cells. a**, Flow cytometric analysis of CD107a, TNF- $\alpha$ , IFN- $\gamma$ , GZMB, and Perforin expression levels in iNK cells and the same donor-expanded UCB-NK cells after K562 stimulation. **b,c**, ELISA analysis of the secretion of TNF- $\alpha$  (**b**), IFN- $\gamma$  (**b**), GZMB (**c**), and Perforin (**c**) in iNK cells and the same donor-expanded UCB-NK cells after K562 stimulation ( $n = 4$  in each group).

Data were presented as mean  $\pm$  SD of four technical repeats from the same experimental unit, representative of two independent experiments.  $P$  values were calculated using unpaired two-sided  $t$ -test. Exact  $P$  values are labelled. **d**, Flow cytometric analysis of typical NK receptors and effectors (CD319, NKp30, NKp44, NKG2D, CD69, CD94, NKG2A, CD96, TRAIL, FasL) in iNK cells, CD19 CAR-iNK cells, and the same donor-generated CD19 CAR-UCB-NK cells.



**Extended Data Fig. 7 | The CD19 CAR-iNK cell showed similar anti-tumor ability compared with the same donor-generated CD19 CAR-UCB-NK cells in NALM6 xenograft animals.** **a**, Schematic diagram of evaluating the cytotoxicities of CD19 CAR-iNK cells and CD19 CAR-UCB-NK cells *in vivo*. **b**, BLI analysis of the xenograft models ( $n = 5$  in each group). **c**, Statistical analysis of total flux (photons/second, p/s) in xenograft models ( $n = 5$  in each group). **d**, Representative FACS plots showing the proportion of human CD45<sup>+</sup>CD56<sup>+</sup> cells from PB in tumor-bearing mice on Day 10. **e**, Statistical analysis of CD45<sup>+</sup>CD56<sup>+</sup>

peripheral blood NK cell ratios in tumor-bearing mice on Day 10 and Day 20 ( $n = 5$  in each group). **f**, Kaplan-Meier survival curves for xenograft models ( $p < 0.001$ , Log-rank test). Data are presented as mean  $\pm$  SD of five mice in each group from the same experimental unit (**c**, **e**, and **f**), representative of two independent experiments.  $P$  values were calculated using the two-way ANOVA test with Tukey's multiple comparisons test or Bonferroni post-hoc test (**c**), or the one-way ANOVA test with Tukey's multiple comparisons test (**e**). Exact  $P$  values are labelled.



Reporting Summary

Nature Portfolio wishes to improve the reproducibility of the work that we publish. This form provides structure for consistency and transparency in reporting. For further information on Nature Portfolio policies, see our [Editorial Policies](#) and the [Editorial Policy Checklist](#).

Statistics

For all statistical analyses, confirm that the following items are present in the figure legend, table legend, main text, or Methods section.

n/a	Confirmed
<input type="checkbox"/>	<input checked="" type="checkbox"/> The exact sample size ( <i>n</i> ) for each experimental group/condition, given as a discrete number and unit of measurement
<input type="checkbox"/>	<input checked="" type="checkbox"/> A statement on whether measurements were taken from distinct samples or whether the same sample was measured repeatedly
<input type="checkbox"/>	<input checked="" type="checkbox"/> The statistical test(s) used AND whether they are one- or two-sided <i>Only common tests should be described solely by name; describe more complex techniques in the Methods section.</i>
<input type="checkbox"/>	<input checked="" type="checkbox"/> A description of all covariates tested
<input type="checkbox"/>	<input checked="" type="checkbox"/> A description of any assumptions or corrections, such as tests of normality and adjustment for multiple comparisons
<input type="checkbox"/>	<input checked="" type="checkbox"/> A full description of the statistical parameters including central tendency (e.g. means) or other basic estimates (e.g. regression coefficient) AND variation (e.g. standard deviation) or associated estimates of uncertainty (e.g. confidence intervals)
<input type="checkbox"/>	<input checked="" type="checkbox"/> For null hypothesis testing, the test statistic (e.g. <i>F</i> , <i>t</i> , <i>r</i> ) with confidence intervals, effect sizes, degrees of freedom and <i>P</i> value noted <i>Give P values as exact values whenever suitable.</i>
<input checked="" type="checkbox"/>	<input type="checkbox"/> For Bayesian analysis, information on the choice of priors and Markov chain Monte Carlo settings
<input checked="" type="checkbox"/>	<input type="checkbox"/> For hierarchical and complex designs, identification of the appropriate level for tests and full reporting of outcomes
<input type="checkbox"/>	<input checked="" type="checkbox"/> Estimates of effect sizes (e.g. Cohen's <i>d</i> , Pearson's <i>r</i> ), indicating how they were calculated

Our web collection on [statistics for biologists](#) contains articles on many of the points above.

Software and code

Policy information about [availability of computer code](#)

Data collection	The flow-cytometry data: LSRFortessa™ X-20 (BD Biosciences), BD FACSAria™ Fusion Flow Cytometer (BD Biosciences).Cell number data: Countstar (Countstar Rigel S2), scRNA-seq data: Chromium system (10 × Genomics, PN120263), Bioluminescence Imaging data: IVIS® Spectrum Imaging System(PerkinElmer), ELISA data:BioTek Synergy H1, Vector copy number data: CFX Opus 96 Real-Time PCR System Bio-Rsd
Data analysis	FlowJo™ Software (v10.8.1) was used for flow-cytometry data analysis. Prism (v9, Graphpad) were used for statistical analysis and plotting. SPSS (version 23, IBM Corp., Armonk, NY, USA) was used for statistical analysis. CellRanger (v6.0.0) and Seurat package (v3.2.3) were used for scRNA-seq data analysis. Living Image® software (v4.4) was used for bioluminescence Imaging data analysis.

For manuscripts utilizing custom algorithms or software that are central to the research but not yet described in published literature, software must be made available to editors and reviewers. We strongly encourage code deposition in a community repository (e.g. GitHub). See the Nature Portfolio [guidelines for submitting code & software](#) for further information.

## Data

Policy information about [availability of data](#)

All manuscripts must include a [data availability statement](#). This statement should provide the following information, where applicable:

- Accession codes, unique identifiers, or web links for publicly available datasets
- A description of any restrictions on data availability
- For clinical datasets or third party data, please ensure that the statement adheres to our [policy](#)

Single-cell RNA sequencing data (UCB-NK, iNK, and CD19 CAR-iNK) (fastq files) have been uploaded to the public database of the Genome Sequence Archive (HRA007978) (<https://ngdc.cncb.ac.cn/gsa-human/browse/HRA007978>). Single-cell RNA sequencing data (iPSC-iNK, ESC-iNK) were downloaded from the Genome Sequence Archive (HRA001609) (<https://ngdc.cncb.ac.cn/gsa-human/browse/HRA001609>). The main data supporting the results in this study are available within the paper and its Supplementary Information. The corresponding author (Jinyong Wang) will make raw data and step-by-step protocols available upon request. Source data for the figures are provided with this paper.

## Research involving human participants, their data, or biological material

Policy information about studies with [human participants or human data](#). See also policy information about [sex, gender \(identity/presentation\), and sexual orientation](#) and [race, ethnicity and racism](#).

Reporting on sex and gender

Sex and gender are not considered in the design of this study

Reporting on race, ethnicity, or other socially relevant groupings

No groupings by race, ethnicity or socioeconomic status were performed.

Population characteristics

Patient #1  
Collection data: 9/26/2023  
Age: 66  
Diagnosis: Follicular lymphoma  
Patient #2  
Collection data: 10/21/2023  
Age: 28  
Diagnosis: B cell-acute lymphoblastic leukemia  
Patient #3  
Collection data: 10/30/2023  
Age: 55  
Diagnosis: B cell-acute lymphoblastic leukemia  
Patient #4  
Diagnosis: B cell-acute lymphoblastic leukemia  
Age: 11

Recruitment

The clinical umbilical cord blood units were obtained from the Guangdong Umbilical Cord Blood Bank (Guangzhou, China). All patient samples were collected with prior consent signatures from the patient and reviewed and approved by the ethics committee of the Jinan University First Affiliated Hospital and the Ethics Committee of Institute of Hematology, Blood Diseases Hospital, CAMS & PUMC.

Ethics oversight

The clinical umbilical cord blood units were obtained from the Guangdong Umbilical Cord Blood Bank (Guangzhou, China) without identification information under province and state regulations. All patient samples were collected at the Jinan University First Affiliated Hospital and Institute of Hematology, Blood Diseases Hospital, CAMS & PUMC from consented patients, and the protocol was approved by the ethics committee of the Jinan University First Affiliated Hospital and the Ethics Committee of Institute of Hematology, Blood Diseases Hospital, CAMS & PUMC.

Note that full information on the approval of the study protocol must also be provided in the manuscript.

## Field-specific reporting

Please select the one below that is the best fit for your research. If you are not sure, read the appropriate sections before making your selection.

☒ Life sciences ☐ Behavioural & social sciences ☐ Ecological, evolutionary & environmental sciences

For a reference copy of the document with all sections, see [nature.com/documents/nr-reporting-summary-flat.pdf](https://nature.com/documents/nr-reporting-summary-flat.pdf)

## Life sciences study design

All studies must disclose on these points even when the disclosure is negative.

Sample size

For all studies, sample size was defined on the basis of our previous studies (Doi.org/10.1038/s41421-022-00467-2, DOI: 10.1111/cpr.13683). Sample sizes for the in vivo experiments were determined empirically on the basis of results from prior publications mentioned above,

	selecting appropriate numbers to achieve statistical significance while minimizing the number of mice used in accordance with the 3 Rs of animal use
Data exclusions	No data were excluded.
Replication	All experiments were performed independently. Replicates of each individual experiment was stated in its figure legends.
Randomization	The clinical umbilical cord blood units were randomly used for induction experiments. All mice received tumor cells at Day-1 then were randomized to split into different groups prior therapeutic cells injection.
Blinding	Experiments were not performed in a blinded fashion. All data were analyzed by software with objective standard.

## Reporting for specific materials, systems and methods

We require information from authors about some types of materials, experimental systems and methods used in many studies. Here, indicate whether each material, system or method listed is relevant to your study. If you are not sure if a list item applies to your research, read the appropriate section before selecting a response.

### Materials & experimental systems

n/a	Involved in the study
<input type="checkbox"/>	<input checked="" type="checkbox"/> Antibodies
<input type="checkbox"/>	<input checked="" type="checkbox"/> Eukaryotic cell lines
<input checked="" type="checkbox"/>	<input type="checkbox"/> Palaeontology and archaeology
<input type="checkbox"/>	<input checked="" type="checkbox"/> Animals and other organisms
<input checked="" type="checkbox"/>	<input type="checkbox"/> Clinical data
<input checked="" type="checkbox"/>	<input type="checkbox"/> Dual use research of concern
<input checked="" type="checkbox"/>	<input type="checkbox"/> Plants

### Methods

n/a	Involved in the study
<input checked="" type="checkbox"/>	<input type="checkbox"/> ChIP-seq
<input type="checkbox"/>	<input checked="" type="checkbox"/> Flow cytometry
<input checked="" type="checkbox"/>	<input type="checkbox"/> MRI-based neuroimaging

## Antibodies

### Antibodies used

Human TruStain FcXTM (Biolegend, clone 422302, cat# 422302), Human CD3-biotin (Biolegend, clone HIT3a, cat# 300304), Human CD3-APC (Biolegend, clone HIT3a, cat# 300312), Human CD7-PerCP-Cy5.5 (Biolegend, clone CD7-6B7, cat# 343116), Human CD16-PerCP-Cy5.5 (Biolegend, clone 3G8, cat# 302028), Human CD19-PE (Biolegend, clone HIB19, cat# 302208), Human CD34-PE (Biolegend, clone 581, cat# 343506), Human CD45-APC-Cy7 (Biolegend, clone HI30, cat# 304014), Human CD45-BV785 (Biolegend, clone HI30, cat# 304048), Human CD56-PE (Biolegend, clone HCD56, cat# 318306), Human CD56-APC (Biolegend, clone HCD56, cat# 318310), Human CD319-PE (Biolegend, clone 162.1, cat# 331806), Human NKp30-BV421 (Biolegend, clone P30-15, cat# 325228), Human NKp44-PE-Cy7 (Biolegend, clone P44-8, cat# 325116), Human NKG2D-APC-Cy7 (Biolegend, clone 1D11, cat# 320824), Human CD69-PE (Biolegend, clone FN50, cat# 310906), Human CD94-BV786 (BD Biosciences, clone HP-3D9, cat# 743953), Human NKG2A-PE (Biolegend, clone S19004C, cat# 375104), Human CD96-PE (Biolegend, clone NK92.39, cat# 338406), Human TRAIL-PE-Cy7 (Biolegend, clone RIK-2, cat# 308216), Human FasL-BV421 (Biolegend, clone NOK-1, cat# 306412), Human CD107a-PE (Biolegend, clone H4A3, cat# 328608), Human CD107a-PE-Cy7 (Biolegend, clone H4A3, cat# 328618), Human TNF- $\alpha$ -BV786 (Biolegend, clone MAb11, cat# 502948), Human IFN- $\gamma$ -PE (Biolegend, clone 4S.B3, cat# 502509), Human Perforin-PerCP-Cy5.5 (Biolegend, clone dG9, cat# 308114), Human GZMB-BV421 (Biolegend, clone QA18A28, cat# 396414), Human 2B4-PerCP-Cy5.5 (Biolegend, clone C1.7, cat# 329516), Human DNAM-1-PE-Cy7 (Biolegend, clone 11A8, cat# 338316), Human NKp46-APC-Cy7 (Biolegend, clone 9E2, cat# 331950), anti-FMC63 scFv-APC (BioSwan, clone M19H, cat# 200102), and anti-FMC63 scFv-biotin (BioSwan, clone CAR Ab, cat# 500014). PE/Cyanine7 anti-human CD161 (Biolegend, clone W18070C, cat#307506), PE anti-human CD328 (Siglec-7) (Biolegend, clone S7.7, cat# 347703), PE anti-human CD279 (PD-1) (Biolegend, clone EH12.2H7, cat# 329906), PerCP/Cyanine5.5 anti-human CD366 (Tim-3) (Biolegend, clone F38-2E2, cat# 345016), APC anti-human TIGIT (VSTM3) (Biolegend, clone A15153G, cat# 372705), PE anti-human CD158a (KIR2DL1) (Biolegend, clone HP-DM1, cat# 374904), PerCP/Cyanine5.5 anti-human CD158e1 (KIR3DL1, NK81) (Biolegend, clone DX9, cat# 312718), and BD Pharmingen™ Alexa Fluor® 647 Mouse Anti-Human KIR2DS4 (CD158i) (BD, clone 179315, cat# 564375). FITC anti-human CD158b/j (KIR2DL2/L3/S2) Antibody (Biolegend, clone DX27, cat# 312604 )

### Validation

All the antibodies used are from commercial sources and have been validated by the vendors. Validation data are available on the manufacturer's website. Antibodies were used according to manufacturer recommendations and gated based on known negative (such as FMO or secondary only) controls. At first use, the antibody volumes used in experiments were tested on positive samples to verify reactivity.

## Eukaryotic cell lines

Policy information about [cell lines and Sex and Gender in Research](#)

### Cell line source(s)

AFT024 (ATCC, SCRC-1007), OP9 (ATCC, CRL-2749), K562 (ATCC, CCL-243), HL-60 (ATCC, CCL-240), Nalm-6 (kindly provided by Professor Min Wang (Leukemia Centre, Institute of Hematology and Blood Diseases Hospital, Chinese Academy of Medical Sciences, Tianjin, China)). A1847 (Honsun Biological Technology Co., Ltd., 36404-89-4 ), MOLM-13 (kindly provided by Professor Hui Cheng (Leukemia Centre, Institute of Hematology and Blood Diseases Hospital, Chinese Academy of Medical Sciences, Tianjin, China), THP-1 (ATCC, TIB-202), 293T (ATCC, CRL-3216), HeLa (Pricella, CL-0101).

### Authentication

The American Type Culture Collection (ATCC), Honsun Biological Technology Co., Ltd. and Pricella uses morphology,



Authentication	karyotyping, PCR and STR assays to authenticate cell lines mentioned above. Morphology and properties pertinent to the experiments as antigens expression were confirmed routinely by flow cytometry.
Mycoplasma contamination	All lines were routinely tested for mycoplasma contamination by qPCR (HZSKBIO®), Mycoplasma DNA Extraction Kit (2G), 1509840-E, Mycoplasma DNA Detection Kit (2G), 1509841-E) and found to be negative.
Commonly misidentified lines (See <a href="#">ICLAC</a> register)	No commonly misidentified cell lines were used.

## Animals and other research organisms

Policy information about [studies involving animals](#); [ARRIVE guidelines](#) recommended for reporting animal research, and [Sex and Gender in Research](#)

Laboratory animals	Species: mouse, strain: NOD/ShiLtJGpt-Prkdcem26Cd52Il2rgem26Cd22/Gpt (NCG); NOD.CB17-PrkdcscidIl2rgtm1Bcgen/Bcgen (B-NDG); NOD.CB17-Prkdcscid Il2rgtm1Bcgen Il15tm1(IL15)Bcgen/Bcgen (B-NDG hIL15), age: 8-10 weeks.
Wild animals	The study did not involve the use of wild animals.
Reporting on sex	8-10 weeks old female mice were used for in vivo tumor-killing assays.
Field-collected samples	This study did not involve field-collected samples.
Ethics oversight	All mice were housed in SPF-grade animal facilities at the Guangzhou Institutes of Biomedicine and Health, Chinese Academy of Sciences and the SPF-grade animal facility of the Institute of Zoology, Chinese Academy of Sciences. All animal-related procedures in this study received approval from the Institutional Animal Care and Use Committee of the Guangzhou Institutes of Biomedicine and Health and the Institutional Animal Care and Use Committee of the Institute of Zoology, Chinese Academy of Sciences. NK cell antitumor activity assessments in animals received approval from the Biomedical Research Ethics Committee of the Guangzhou Institutes of Biomedicine and Health, Chinese Academy of Sciences and the Biomedical Research Ethics Committee of the Institutional Animal Care and Use Committee of the Institute of Zoology, Chinese Academy of Sciences.

Note that full information on the approval of the study protocol must also be provided in the manuscript.

## Plants

Seed stocks	n/a
Novel plant genotypes	n/a
Authentication	n/a

## Flow Cytometry

### Plots

Confirm that:

- ☒ The axis labels state the marker and fluorochrome used (e.g. CD4-FITC).
- ☒ The axis scales are clearly visible. Include numbers along axes only for bottom left plot of group (a 'group' is an analysis of identical markers).
- ☒ All plots are contour plots with outliers or pseudocolor plots.
- ☒ A numerical value for number of cells or percentage (with statistics) is provided.

### Methodology

Sample preparation	Flow cytometry analysis of CD34+ HSPC cells and CD19-CAR CD34+ HSPC cells: The clinical umbilical cord blood units for CD34+HSPC isolation or NK cell expansion were obtained from the Guangdong Umbilical Cord Blood Bank (Guangzhou, China). Mononuclear cells were isolated from umbilical cord blood using ficoll. CD34+ cells were enriched from mononuclear cells using the CD34 Isolation Kit (Miltenyi). CD19-CAR CD34+ HSPC were generated by infecting with CD19 CAR retroviruses using Vectofusin®-1 (Miltenyi). CD34+ HSPC cells and CD19-CAR CD34+ HSPC cells were stained with the destined antibodies (human CD45, CD34, Anti-Mouse FMC63 scFv Monoclonal Antibody) in FACS buffer (2% FBS, DPBS) for 30min on ice avoiding exposure to light. After incubation, cells were centrifugated (500g, 5min) and the supernatants were discarded. DAPI solution was used for resuspending the cells to label dead cells. Flow cytometry analysis or sorting of iNK cells, CD19-CAR iNK cells, UCB-NK cells and primary tumor cells:
--------------------	--

iNK cells and CD19-CAR iNK cells were generated using the three-step induction method. CD3 negative cells were isolated from CD34 negative cells by depletion of CD3 positive cells using Biotin anti-human CD3 Antibody (BioLegend) and anti-Biotin MicroBeads (Miltenyi). NK cells were expanded from the CD3 negative cells using K562-mIL21 cells (Hangzhou Zhongying Biomedical Technology Co., Ltd.). ovarian tumor-bearing mice were sacrificed by cervical dislocation. Peritoneal cells from peritoneal cavity were collected using PBS by syringe (5 mL). Peripheral blood cells (mouse) were harvested from B cell tumor-bearing mouse via standard eye bleed protocol. Red blood cells were removed by ammonium-chloride-potassium (ACK). Primary patient B cell lymphoma tissues were mechanically separated into 1 mm × 1 mm fragments. tumor cells were isolated by digesting the fragments using digestion buffer (1 mg/ml Collagenase type IV, 1 mg/ml Dispase, and 50 U DNase I). Primary patient B cells were isolated using Ficoll. Primary tumor cells were stained with CD19 antibody to determine the ratio of CD19 positive cells. Cells were stained with the destined antibodies which have a detailed description in method according to the manufacturers' instructions. DAPI solution was used for resuspending the cells to label dead cells.

Tumor cells for Killing assay in vitro:

tumor cells from cell lines or patients were labeled with eBioscience™ Cell Proliferation Dye eFluor™ 670 (eBioscience) or carboxyfluorescein diacetate succinimidyl ester (CFSE; Beijing BioRab Technology Co. Ltd) before incubating with effectors (E). The number of tumor cells (Target, T) and effectors were determined by the Countstar, followed incubation at the designed E/T ratios. The incubated cells were stained with DAPI solution before FACS analysis.

Flow cytometry analysis of TNF $\alpha$ , IFN- $\gamma$ , Perforin, and GZMB:

iNK cell and UCB-NK cells were first stained with anti-human CD56. Fixation and permeabilization were performed using the FIX & PERM Kit (MULTISCIENCES), followed by intracellular staining for TNF- $\alpha$ , IFN- $\gamma$ , Perforin, and GZMB according to the manufacturers' instructions.

Instrument	Manual MACS® Magnetic Separators (Miltenyi), Countstar (Countstar Rigel S2), LSRFortessa™ X-20 (BD Biosciences), BD FACSAria™ Fusion Flow Cytometer (BD Biosciences).
Software	FlowJo™ Software (v10.8.1)
Cell population abundance	The purity of the analysed primary samples was confirmed by flow cytometry
Gating strategy	Cells were gated on (1) SSC-A vs. FSC-A, selecting the major cell population, (2) FSC-W vs. FSC-A, selecting single cells based on the visible population distribution, (3) Excepted for cells for intracellular proteins analysis, live cells based on negative staining for DAPI solution, and then (4) subsequent stains dependent on the panel of interest. Exemplary gating strategies are provided in Extended Data Fig. 1B.

☒ Tick this box to confirm that a figure exemplifying the gating strategy is provided in the Supplementary Information.